

Article

Hydrometeorological and Socio-Economic Impact Assessment of Stream Flooding in Southeast Mediterranean: The Case of Rafina Catchment (Attica, Greece)

Christos Giannaros ^{1,2,*}, Vassiliki Kotroni ² , Konstantinos Lagouvardos ²,
Christina Oikonomou ¹, Haris Haralambous ^{1,3} and Katerina Papagiannaki ² 

¹ Frederick Research Center, Pallouriotissa, Nicosia 1036, Cyprus; res.ec@frederick.ac.cy (C.O.); eng.hh@frederick.ac.cy (H.H.)

² National Observatory of Athens, Institute for Environmental Research and Sustainable Development, Palea Penteli, 15236 Athens, Greece; kotroni@noa.gr (V.K.); lagouvar@noa.gr (K.L.); katpap@noa.gr (K.P.)

³ Department of Electrical Engineering, Frederick University, Pallouriotissa, Nicosia 1036, Cyprus

* Correspondence: res.gc@frederick.ac.cy

Received: 4 July 2020; Accepted: 27 August 2020; Published: 29 August 2020



Abstract: The CyFFORS (Cyprus Flood Forecasting System) project aims at increasing flood risk awareness and promoting preparedness against flooding by developing and validating a pilot flood forecasting system targeted over three river/stream basins in the Larnaca region, Cyprus, and Attica region, Greece. The present study demonstrates the analysis of flood-associated information, based on ground-based and ERA5 model reanalysis data, which is a necessary procedure prior to the development of the hydrometeorological modeling tool, in one of the study areas, namely in the Rafina catchment in Attica, Greece. The analysis focusses on 12 stream flood episodes that occurred in the period 2008–2014. The results show that most events were associated with a typical, for the study area, wet-season cyclonic activity. The detailed investigation of two case studies highlighted important spatiotemporal differences in the generation and development of rainfall, as well as in the flooding magnitude, which were related to specific characteristics of the synoptic-scale forcing, topography and soil moisture preconditioning. Moreover, highly correlated positive relationships were found between the observed maximum stream discharge and the duration and maximum total accumulation of precipitation. A strong positive correlation was also evident between the peak discharge and the flooding impacts, leading to the identification of preliminary discharge thresholds for impact-based warnings, which can be applied to the pilot CyFFORS forecasting system.

Keywords: high-impact rainfall events; flooding; hydrometeorological analysis; socio-economic impacts; ground-based data; ERA5 model reanalysis; Greece; Mediterranean

1. Introduction

Flood-associated events, including river/stream floods, triggered by heavy precipitation are among the most frequent weather-related hazards [1] affecting, substantially, the natural and human environment. Their impact can be dramatic, as extreme episodes may cause multiple fatalities and massive economic losses due to damage to private properties, public structures and utilities. For instance, the catastrophic flash flood of 17 November 2017 in Mandra, West Attica, Greece, caused by an intense storm that led two small impermanent streams in the area to overflow, resulted in 24 reported deaths and in widespread material damages across the town [2–4]. The European continent has experienced a considerable number of similar high-impact flood episodes over the last decades [5–7], especially

in the Mediterranean region in recent years [8–11], due to the local climate and complex topography that favor severe rainfall events [12–14]. Future climate projections demonstrate that the number of days and severity of extreme precipitation are likely to increase despite decreases in total annual and seasonal rainfall [15]. This fact, combined with rising urbanization and economic growth, is expected to make river/stream floods more frequent, intense and damaging in terms of human casualties and financial losses [16–19]. However, since these changes deviate strongly at the regional level, addressing the river/stream flood risk in each country is essential.

The Cyprus Flood Forecasting System (CyFFORS) project, a joint initiative between Cyprus and Greece, aims at contributing to this direction by increasing risk awareness and promoting preparedness against river/stream flooding at a local level in Cyprus and Greece. To achieve this goal, a pilot flood forecasting system targeted over three river/stream basins in two highly susceptible to flooding regions (Larnaca in Cyprus and Attica in Greece) will be developed and validated. The forecasting system will be based on the Weather Research and Forecasting (WRF) model coupled with its hydrological (Hydro) extension package (WRF-Hydro; [20,21]). Many studies implemented with the use of the WRF-Hydro model demonstrated its capability in providing precise and in-depth spatiotemporal information on fluvial floods in terms of hindcasting [4,10,22,23], operational forecasting [24–26] and climate research [27,28]. Prior to the development of the WRF-Hydro-based river inundation modeling system in Larnaca, Cyprus, and Attica, Greece, the description of the status regarding flood dynamics and impact in the studied areas is a fundamental step. For instance, Borga et al. [29] investigated a storm event that occurred in August 2003 on the upper Tagliamento river basin in the eastern Italian Alps as a prototype mesoscale convective system that was likely responsible for the majority of flash flood peaks in the basin. One of their principal outcomes was the significant role of the antecedent soil moisture distribution, as well as the storm structure, motion and evolution in the flood response. Similarly, Delrieu et al. [30] documented the hydrometeorological characteristics of the September 2002 catastrophic flash flood in Gard region, France, highlighting the influence of the spatiotemporal rainfall pattern and geomorphological factors on the hydrological response of the area's watersheds. The same flood event was studied by Ruin et al. [31], who incorporated an analysis of human casualties into their investigation, showing that the small Gard region catchments are the most dangerous in both hydrological and risk to life terms. Moreover, Pino et al. [32] conducted a hydrometeorological analysis of substantial floods in three hydroclimatic units in the NE Iberian Peninsula identifying a major synoptic pattern associated with the floods, as well as a high positive relationship between atmospheric instability and maximum specific peak flows. Similarly, Greco et al. [33] combined ground-based observations and large-scale modeling products to identify and study the synoptic fields associated with the rainfall patterns in Calabria region (Italy), giving special emphasis on very extreme episodes. Their analysis allows for improving the predictability of rainfall-related phenomena and the design of damaging event scenarios, considering extraordinary extreme episodes, the characterization of which is of particular interest in flood management, as they occur at small spatiotemporal scales and at high return periods (i.e., they have low frequency of occurrence), inducing severe impacts to society [34]. Furthermore, Romang et al. [35] showed that the analysis of precipitation data of previous floods during the early development stage of a flood warning system was useful for defining primary flood-related thresholds and evaluating the hazard potential of future events. Thus, the analysis of the hydrometeorological characteristics of past floods contributes substantially to our knowledge about large-scale and regional flooding drivers and mechanisms, assisting floods' attribution, forecasting and risk mitigation [29,30,32–35]. Also, investigating the flooding river/stream discharges in relation to their influence on people, properties and infrastructures is crucial for understanding the social aspects involved in flooding [31] and for implementing impact-based early warning systems and, consequently, expanding the flood forecasting chain to include the potential effects and losses [36,37].

Considering the above, the current paper provides a hydrometeorological and socio-economic impact assessment of 12 floods that occurred in the past two decades in one of the CyFFORS targeted watersheds, namely in the Rafina stream basin in Attica, Greece. The assessment was conducted

combining ground-based hydrometeorological observations, ERA5 model reanalysis data [38] and socio-economic impact reports and records. The analysis includes the examination of the synoptic atmospheric conditions and lightning activity associated with the identified stream floods. Each episode is characterized concerning rainfall duration and severity in terms of 1-h and total accumulation, and maximum stream discharge. Moreover, an impact intensity categorization is introduced to classify the flood-induced socio-economic impacts and investigate their link to the peak stream discharges. Finally, a case study analysis that includes the examination of soil moisture conditions is presented for two events representing different synoptic, hydrometeorological and soil moisture conditions, and different resulting impact.

2. Materials and Methods

2.1. Study Area and Data Sources

Among the CyFFORS targeted watersheds, the Rafina stream basin was selected for the purpose of the present study due to the sufficient flood-related data availability that characterizes the area in terms of both hydrometeorological and socio-economic impact information. The Rafina drainage network is part of the GR06RAK0003 potentially significant flood risk (PSFR) zone (Figure 1b), which was defined by the Greek Special Secretariat for Water (SSW; [39]) under the European Council (EC) Floods Directive 2007/60/EC [40]. It is situated in East Attica (Figure 1a) and covers 123 km². It includes residential areas of the Rafina-Pikermi, Penteli, Pallini, Peania and Spata regions with a total population coverage of ~85,000 residents. Concerning geomorphology, the area comprises of Mount Penteli to the north, the Spata plain to the south and Mount Hymettus to the southwest, while it is open to the sea (Euboean Gulf) from the east (Figure 1b). The Rafina catchment is greatly prone to flooding because of large wildfire burnt territories, increased urbanization, mild topographic slopes and the absence of efficient inundation protection.

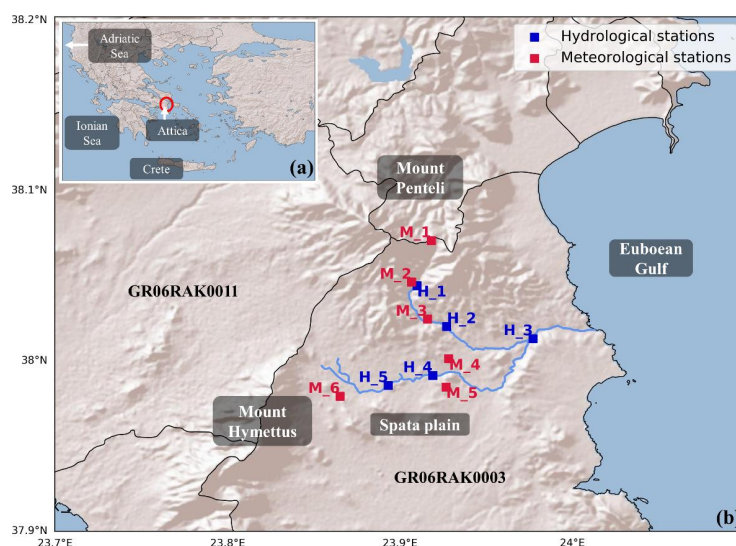


Figure 1. (a) Map of Greece with identification of regions of interest and (b) locations of the ground-based hydrological and meteorological stations with identification of the GR06RAK0003 zone and of the regional and geomorphological features in the Rafina stream basin.

Table 1 presents the main characteristics of the ground-based hydrological and meteorological stations used in the present study. The collected data include measurements of precipitation and stream discharge with 10-min temporal resolution covering the period 2008–2014. The hydrological observations were provided by the Hydrological Observatory of Athens (HOA) of the National and Technical University of Athens (NTUA) in five stations, while the precipitation observations were retrieved from six meteorological stations operated by the National Observatory of Athens (NOA)

and NTUA (Figure 1b). NTUA operates HOA, which consists of 15 meteorological stations and six streamflow measuring sites in Attica region, since 2005. The same year NOA started to build a country-scale network of automated weather stations, which is continuously expanding and currently exceeds 410 stations in Greece. Both NTUA and NOA networks comply with the World Meteorological Organization (WMO) guidelines concerning site selection for stations' installation, monitoring and surveying [41,42]. NOA applies a two-step operational quality control procedure in order to assure that only high-quality data are included in the archive database, from which the rainfall data from Spata_M and Kantza stations were obtained for the purposes of the present study [41]. NTUA provides raw and processed (i.e., containing some corrections) time series of the hydrometeorological measurements through the website of HOA (<http://hoa.ntua.gr/>; [42]). For both types of datasets, the data obtained from the HOA/NTUA database were thoroughly examined in the current study in order to exclude data of questionable quality.

Table 1. Key characteristics of the ground-based observational stations.

Monitoring Network	Station Name	Station ID ¹	Latitude (° N)	Longitude (° E)	Altitude (m a.s.l. ²)
HOA/NTUA	Lykorema	H_1	38.01	23.98	30
	Drafi_H ¹	H_2	37.99	23.92	105
	Rafina	H_3	38.02	23.93	143
	Pikermi_H ¹	H_4	38.04	23.91	286
	Spata_H ¹	H_5	37.98	23.89	137
	Diavasi Balas	M1	38.04	23.91	393
	Ayios Nikolaos	M2	38.02	23.92	203
	Drafi_M ¹	M3	38.00	23.93	133
	Pikermi_M ¹	M4	38.07	23.92	630
NOA	Spata_M ¹	M5	37.98	23.93	144
	Kantza	M6	37.98	23.87	221

¹ H denotes a hydrological station, while M denotes a meteorological station. ² above sea level.

2.2. Flood Episodes Selection

The basis for choosing the fluvial inundation events in the study area was the examination of historical floods in the 2017 SSW report on the Attica PSFR areas [39], as well as of information associated with floods in weather-related databases including: (a) the European Severe Weather Database (ESWD; <https://www.eswd.eu/>) operated by the European Severe Storms Laboratory (ESSL), (b) the Emergency Events Database (EM-DAT; <https://www.emdat.be/>) operated by the Centre for Research on the Epidemiology of Disasters (CRED), (c) the NOA database of high-impact weather events in Greece (<http://stratus.meteo.noa.gr/events>; [9]), and (d) the rainfall events database of HOA/NTUA. This initial investigation resulted in finding thirty-two flood-related incidents between 2004 and 2014. Eighteen of these incidents were considered as significant flood episodes based on the hydrological response intensity of the study catchment. In particular, the peak stream discharge over at least three stations, including always the H_3 site (Figure 1b), which is close to the watershed's outlet, was greater than 10 m³/s for these events. Finally, twelve stream flood episodes were selected considering the meteorological and socio-economic data availability.

2.3. Assessment Process

In order to understand the flood-related physical mechanisms and their relation to impact in the Rafina catchment, the selected flood episodes were classified based on the: (a) associated synoptic atmospheric conditions and lightning activity, (b) observed rainfall duration and severity, (c) observed maximum stream discharge, and (d) intensity of the resulting socio-economic impacts. More specifically, the synoptic meteorological analysis was conducted using the ERA5 surface and upper air reanalysis data at 0.25° × 0.25° spatial and 1 h temporal resolution [43,44] provided by the European Centre for Medium-Range Weather Forecasts (ECMWF), while the lightning activity, which is indicative of the presence of convective motions, during each episode was qualitatively characterized using data from

the ground-based ZEUS lightning detection network operated by NOA (<https://meteo.gr/talos/>; [45,46]). The rainfall duration of each event was defined by examining the observed hydrographs (time-series of precipitation and stream discharge), while the precipitation severity was determined in terms of maximum total and 1-h accumulation of rainfall considering the total and 1-h precipitation accumulations recorded within the event duration at all the available meteorological stations inside the study watershed. The maximum stream discharge for each episode was derived considering the observations obtained from the measuring sites that are close to locations at risk inside the Rafina stream basin (i.e., Rafina, Pikermi_H and Spata_H stations; Table 1). The socio-economic impact analysis was implemented by investigating reports describing the flood damages and effects in the NOA high-impact weather events database [9]. Also, fire service operations in flooded properties provided by the Greek Fire Department were examined [47]. Each event was classified according to four impact intensity categories that were defined based on the classification used by Papagiannaki et al. [9] for the high-impact weather events database in Greece and by the United Kingdom (UK) Flood Forecasting Services [48,49] for their operational flood guidance statement. As shown in Table 2, each impact intensity class considers the type and magnitude of the flood-induced effects. The types of impact include the key effects of flooding on society, i.e., the risk to human life, damage to property (e.g., buildings) and public structures, and the disruption to transport and utilities (e.g., electricity), while the magnitude of impact is associated with the severity and spatial and temporal extent of the effects [9,48,49]. Finally, the investigation of the soil moisture conditions during the analysis of two selected case studies, namely events #4 and #12, was carried out using the ECMWF ERA5 reanalysis land hourly data at $0.1^\circ \times 0.1^\circ$ horizontal grid resolution [50]. The selection of the case events was conducted considering the different atmospheric and soil moisture conditions, as well as the different hydrometeorological and socio-economic impact features, which characterized the episodes.

Table 2. Socio-economic impact intensity classification.

	I0: Minimal	I1: Minor	I2: Significant	I3: Severe
Human life	Not expected	Risk for vulnerable groups of people and/or people involved in endangered situations	Danger to life due to physical hazards associated with flooding water	Danger to life due to physical, chemical and utility hazards associated with flooding water
Damage to properties and public structures	Not expected	Light damage to individual properties	Important damage to many properties and/or public structures	Extensive damage to multiple properties and/or public structures
Transportation	Little or no disruption to river crossings and/or roads close to the river/stream	Small-scale disruption (local and short term)	Large-scale disruption (broad or long term) and/or important damages to the transport network	Extensive disruption (broad and long term) and/or extensive damages to the transport network
Utilities	Not expected	Small-scale disruption (local and short term)	Large-scale disruption (broad or long term)	Extensive disruption (broad and long term) and/or loss of utilities

3. Results

3.1. Hydrometeorological and Socio-Economic Impact Analysis

Table 3 shows that all examined flood events took place during the wet period. This outcome was expected, since heaviest precipitation amounts and greater resulting impact occur during the wet season of a hydrological year compared to the period between May and September [14,51,52]. This is due to the global atmospheric circulation during the autumn and winter, which interacts with the complex geomorphology and land-sea temperature contrast in the Eastern Mediterranean region, favoring the development of cyclonic atmospheric conditions [14,53]. The studied flood episodes were associated with this type of large-scale atmospheric circulation. In particular, the events were driven by low-pressure systems, which, in most cases, affected the area of interest while moving from the west towards the east. The surface low-pressure systems during the majority of the episodes were accompanied by troughs and cut-off lows in the middle troposphere assisting their organization and preservation over Greece (Table 3).

Table 3. Hydrometeorological and impact intensity characteristics of the examined flood episodes.

Event Nb	Dates	Driving Meteorological Mechanism	Lightning Activity	Rainfall Duration (h)	Max Total Rainfall (mm)	Max 1-h Rainfall (mm/h)	Max Discharge (m ³ /s)	Impact Intensity Class	
#1	17 November 2008	Surface low-pressure system accompanied by an upper-level trough	Low	7	49.3	23.7	22.3	I1 (light damage to buildings and localized disruption to transportation)	
#2	25 October 2009		High	15	31.4	16.8	29.7		
#3	3 November 2009		Surface low-pressure system accompanied by an upper-level cut-off low		10	36	16		22
#4	11 December 2009				11	84.6	18.6		25
#5	02 January 2011	Surface low-pressure system accompanied by an upper-level trough		8	32	16.8	17.3	I0 (little or no effects on roads close to the stream)	
#6	3–4 February 2011	Exceptional atmospheric circulation	Low	39	148.6	12.2	79.7	I2 (damage to many properties and public structures, and large-scale disruption to transport networks)	
#7	24–25 February 2011	Surface low-pressure system accompanied by an upper-level cut-off low		19	92.2	26	37.9	I1 (light damage to buildings and localized disruption to transportation)	
#8	6–7 February 2012			11	48.6	21.2	38.0		
#9	29–30 November 2012	Surface low-pressure system associated with extended upper-level troughs	Moderate	8	54.4	37	24.4	I1 (light damage to buildings and localized disruption to transportation)	
#10	29–30 December 2012	Surface low-pressure system accompanied by an upper-level cut-off low		18	209	27	37.3		
#11	16 January 2013	Surface low-pressure system associated with extended upper-level troughs	Low	4	20.8	15	16.6	I0 (little or no effects on roads close to the stream)	
#12	22 February 2013	Surface low-pressure system accompanied by a negatively tilted upper-level trough	High	10	138.8	39.4	152.8	I2 (damage to many properties and public structures, and large-scale disruption to transport networks)	

This is evident in Figures 2–5, which demonstrate the synoptic conditions at approximately the hour of maximum rainfall intensity for each event. During episodes #1 and #5, the surface cyclones were located in the Ionian Sea south of Italy (see location in Figure 1b), affecting the study watershed in combination with upper-level troughs (Figure 2a,b and Figure 3c,d). Similarly, the synoptic circulation during events #9 and #11 was characterized by extended troughs at 500 hPa geopotential height over the study area, associated with deep surface lows, which, in this case, were situated far away from the Rafina catchment west of North Italy (Figure 4e,f and Figure 5c,d). In the course of events #2, #3, #4, #7, #8 and #10, the study stream basin was affected by surface low-pressure systems combined with cut-off lows in the middle troposphere (Figure 2c–f, Figure 3a,b, Figures 4a–d and 5a,b). The systems at the examined hour were found over the Ionian and Adriatic Seas, except during event #4, where the system was situated over Crete in southern Greece (see locations in Figure 1b). As shown in Table 3, most episodes were characterized by low to moderate lightning activity indicating, respectively, low to moderate convective activity.

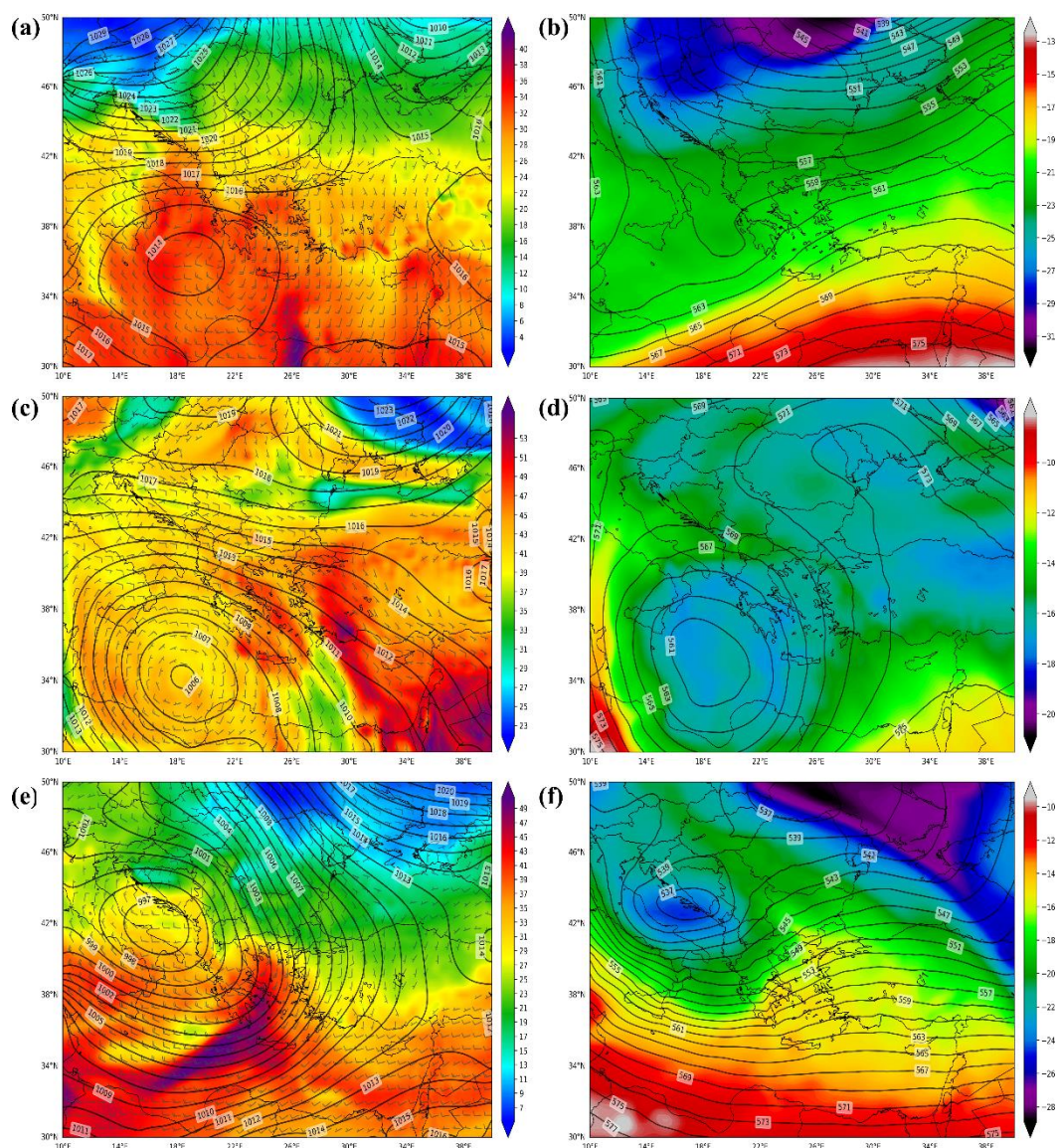


Figure 2. Sea-level pressure (contours; hPa) and 850 hPa equivalent potential temperature (shading; °C) and wind barbs (a,c,e), and 500 hPa air temperature (shading; °C) geopotential height (contours; dm; b,d,f) from the $0.25^\circ \times 0.25^\circ$ ERA5 reanalysis data on 17 November 2008, 1500 UTC (a,b), 25 October 2009, 0900 UTC (c,d), and 3 November 2009, 1500 UTC (e,f).

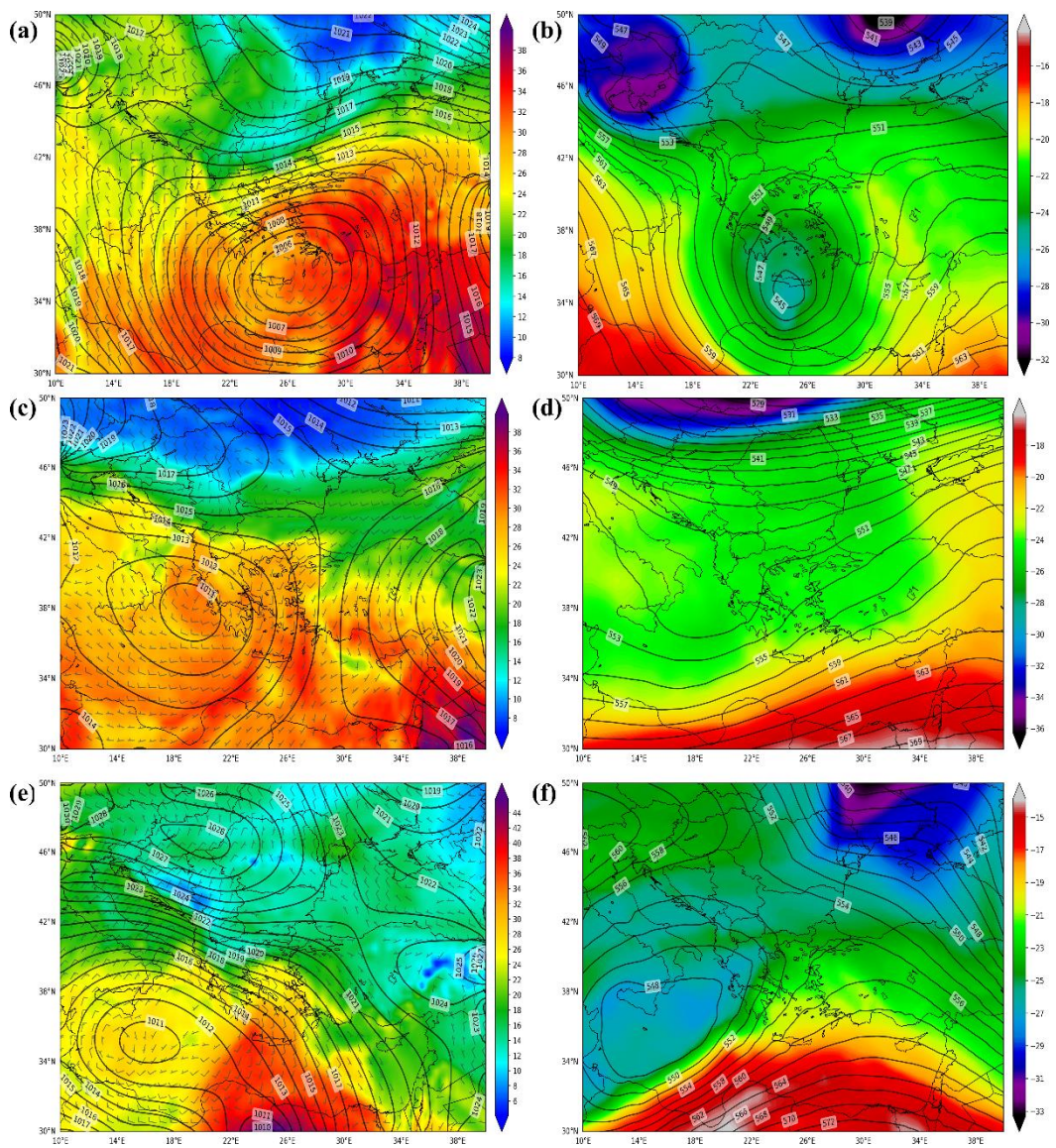


Figure 3. As in Figure 2 but for 11 December 2011, 0400 UTC (a,b), 2 January 2011, 1500 UTC (c,d), and 3 February 2011, 0600 UTC (e,f).

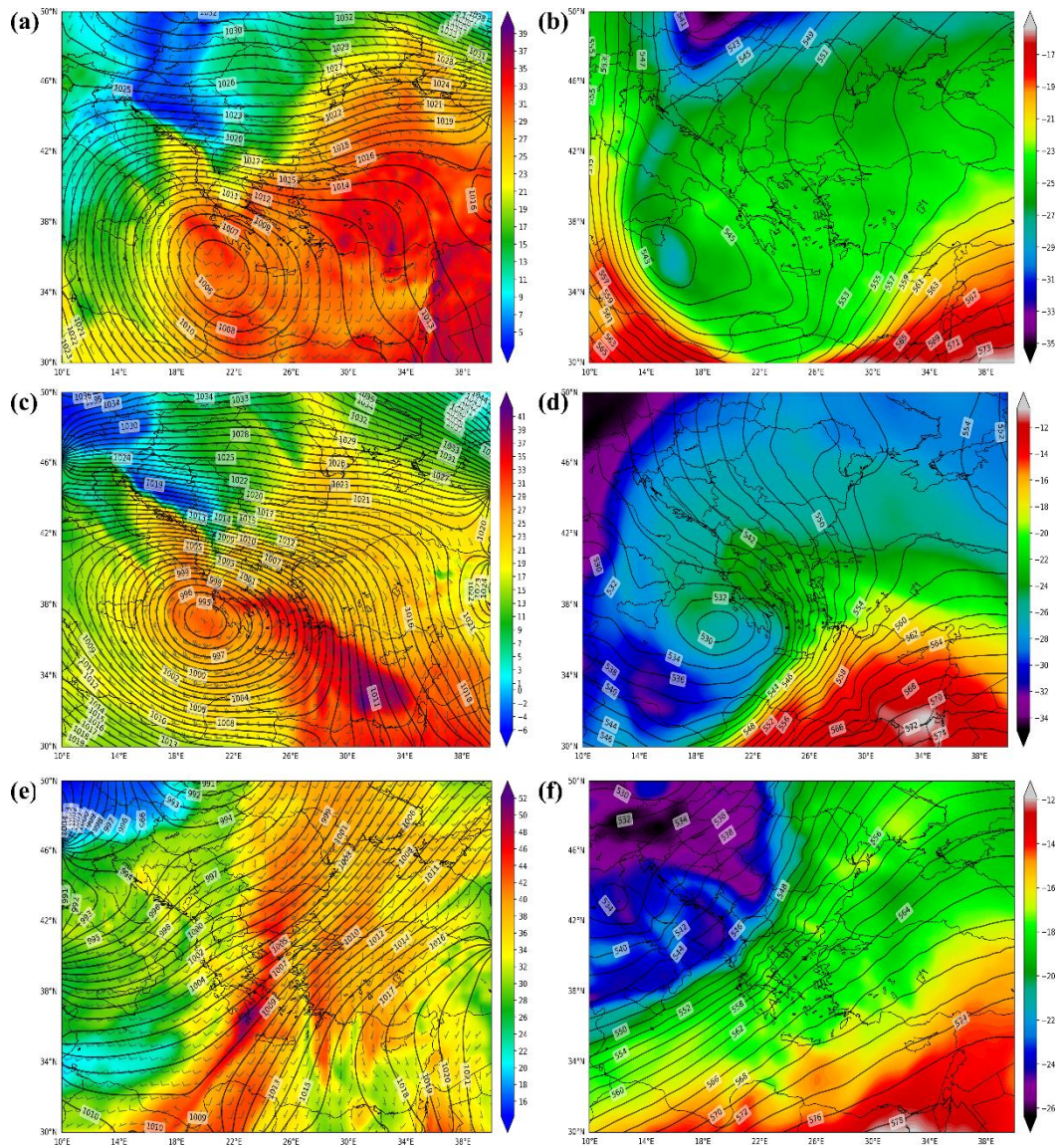


Figure 4. As in Figure 2 but for 24 February 2011, 1200 UTC (a,b), 06 February 2012, 1800 UTC (c,d), and 29 November 2012, 1800 UTC (e,f).

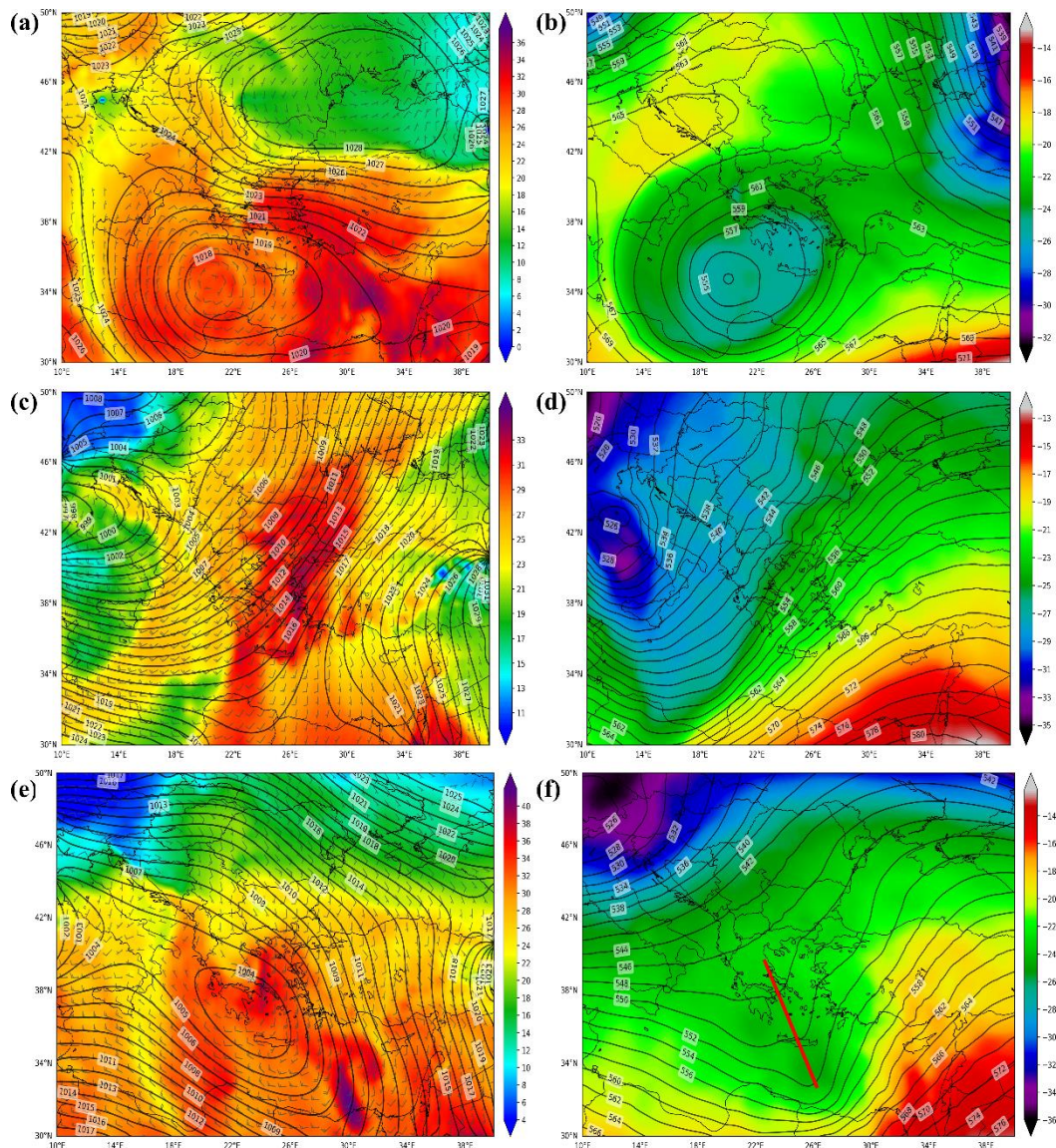


Figure 5. As in Figure 2 but for 30 December 2012, 0900 UTC (a,b), 16 January 2013, 0900 UTC (c,d), and 22 February 2013, 0800 UTC (e,f). The red line in map (f) indicates the negatively tilted trough axis.

The above features represent typical cyclonic activity in Greece [14,54,55], which, in the present analysis, contributed to the advection of warm, humid and highly unstable air masses over the wider area of the Rafina watershed. Consequently, considerable precipitation amounts were produced over the study catchment and a subsequent hydrological response that led mainly to minor impact (I1 impact intensity class) associated with light damage to buildings and localized disruption to transportation (Table 3). In particular, individual properties in the residential areas of the Rafina stream basin were slightly affected during events #1, #3, #4, #7, #8, #9 and #10, while small-scale disruption to transportation in the Penteli region took place in the course of event #2. Significant impact (I2 impact intensity class) concerning many properties and public structures, as well as large-scale disruption to transport networks were induced in the inhabited regions of the Rafina watershed during events #6 and #12. In the first case, an exceptional atmospheric pattern affected Greece (Figure 3e,f) and caused long-lasting and low-intensity rainfall over the study area (Table 3). Event #12 occurred due to the development of a very deep surface cyclone associated with a 500-hPa trough, which exhibited a negative tilt (Figure 5e,f) that led to local instability and, consequently, enhanced convective motions

associated with high lightning activity across the trajectory of the surface low over Greece. As a result, heavy precipitation of short duration was produced over the Rafina catchment (Table 3).

Figure 6 demonstrates that peak stream discharge increases as the duration of rainfall increases. The two variables are highly correlated, as indicated by the nonparametric Spearman coefficient (ρ), which is equal to 0.72 (statistically significant at the 95% confidence interval; * p). A high positive correlation ($\rho = 0.71$), statistically significant at the 95% confidence interval (* p), is also evident for the maximum discharge and total precipitation, whereas the low ρ value (0.32), when the maximum discharge and 1-h rainfall are examined, reveals a weak positive correlation between these parameters (Figure 6). The latter outcome is mainly due to events #6 and #9. When these episodes are excluded from the analysis, the Spearman coefficient between the peak discharge and maximum 1-h precipitation is equal to 0.81 (statistically significant at the 99.9% confidence interval; *** p), showing a strong positive relation between the parameters, with the correlation results for the rest of the variables not being affected significantly (Figure A1). The peak discharge reached up to 80 m³/s approximately during episode #6 despite the fact that it was characterized by the lowest 1-h rain intensity (12.2 mm/h; Table 3). In this case, the ground saturation effect contributed primarily to flooding, with a significant impact (I2 impact intensity class), as denoted by the long rainfall duration (39 h) and the substantial maximum total precipitation (148.6 mm; Table 3). In the course of event #9, the significant accumulation of 1-h precipitation (37 mm) in 8 h (Table 3) led to infiltration excess, contributing to the flood that induced minor impacts (I1 impact intensity class). For event #12, which also led to a significant impact (I2 impact intensity class), high values of maximum total and 1-h rainfall (138.8 mm and 39.4 mm/h, respectively) were recorded in a short period (10 h; Table 3) as a result of the severe convective cloudbursts. Therefore, both saturation and infiltration excess resulted in the intense flood with the maximum stream discharge surpassing 150 m³/s (Table 3).

Peak discharges lower than 20 m³/s are reported for events #5 and #11, which are associated with very low duration and maximum total and 1-h accumulations of precipitation (Figure 6). These events resulted in minimal impact (I0 impact intensity class), i.e., little or no effects on roads close to the stream, while minor impact (I1 impact intensity class), related mainly to individual properties affected, was induced by the rest of the flood episodes, which are characterized by maximum stream discharges that vary between 20 and 40 m³/s (Figure 6). The latter events include episode #10 that produced large amounts of accumulated precipitation, but in considerably lower duration compared to event #6, and episode #9, which led to high maximum 1-h rainfall but with significant lower maximum total precipitation compared to event #12. The analysis illustrated in Figure 6 shows that the socio-economic impact is higher when the peak stream discharge increases, with the two parameters being strongly correlated ($\rho = 0.84$; statistically significant at the 99.9% confidence interval; *** p). This outcome is of great importance as preliminary discharge thresholds for impact-based warnings can be used for the future pilot operational flood forecasting needs in the framework of the CyFFORS project.

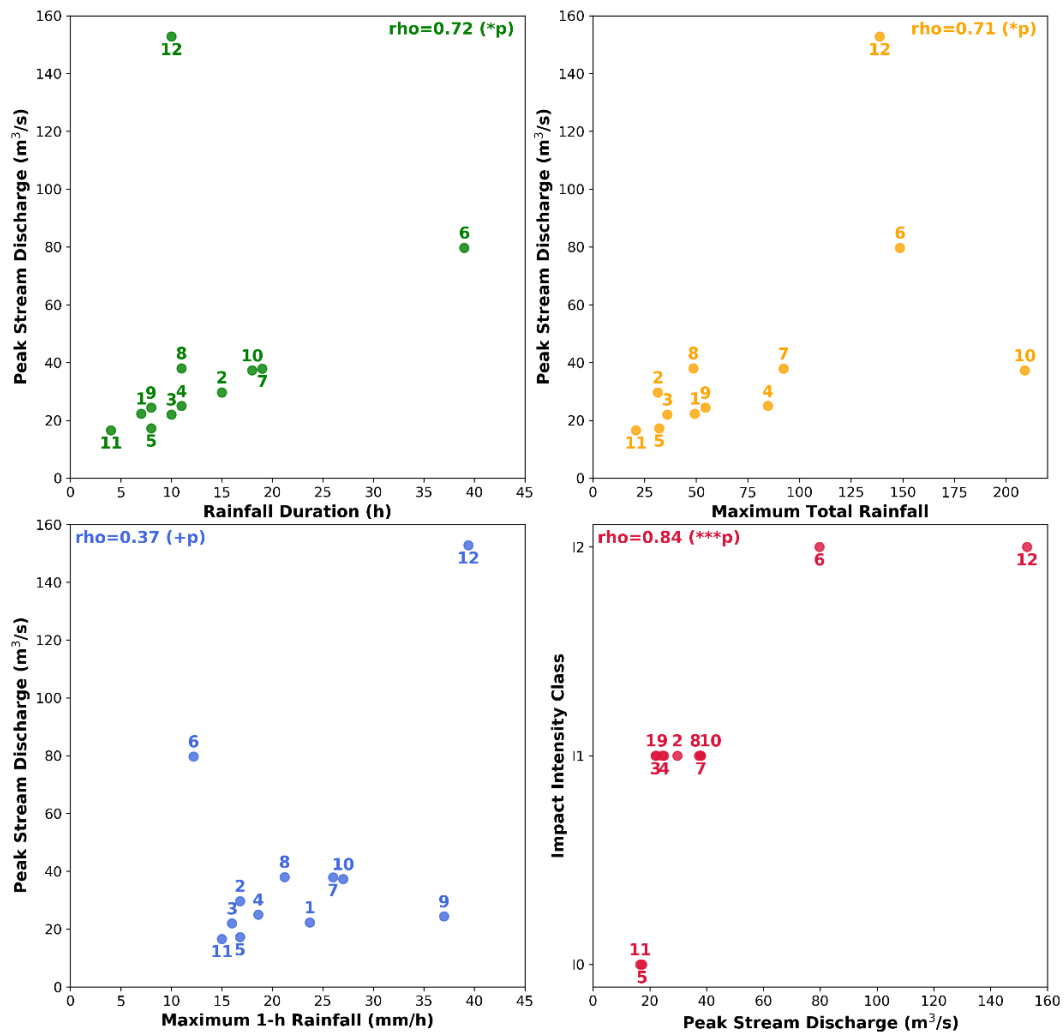


Figure 6. Maximum stream discharge against duration and maximum total and 1-h accumulations of precipitation, and impact intensity against maximum stream discharge. The numbers indicate the events IDs (Table 3), while rho values indicate the Spearman correlation coefficient, with statistical significance, *p* value, being symbolized as: +*p* (>0.05; not significant), * *p* (≤0.05; 95% confidence interval) and *** *p* (<0.001; 99.9% confidence interval).

3.2. Case Studies Analysis

3.2.1. 11 December 2009

The maximum total and 1-h precipitation in the course of flood event #4 was observed at Spata_M (M_5) meteorological station, while the maximum streamflow was recorded at the Rafina hydrological measuring site (see location in Figure 1b). In particular, 84.6 mm were recorded at the M_5 site, located in the plain area of the Rafina stream basin, between 10 December 2009, 2100 UTC to 11 December 2009, 0700 UTC. For the same period, 30–40 mm and 60–70 mm of precipitation were observed at the M_4 and M_6 stations and in the mountainous areas of the catchment (M_1 and M_2 sites), respectively (Figure 7).

Figure 8 shows that rainfall over Spata started on 2050 UTC 10 December and, after a short stop of 50 min, it intensified reaching its 10-min peak (5.2 mm) around midnight. Significant amounts of rain persisted during the first three morning hours of 11 December, while the precipitation ended on 0510 UTC 11 December. The basin-averaged soil moisture prior to the event was equal to ~0.32 m³/m³, gradually increasing during the next hours and reaching up to ~0.39 m³/m³ at 0700 UTC 11 December, due to the occurrence of precipitation in the watershed. The hydrologic response of the catchment at

the Rafina station, characterized by an abrupt increase in stream discharge, occurred 4 h and 20 min after the rainfall's start and was followed by a mild streamflow decline until 0320 UTC 11 December. The persistence of rain and the wetter soil moisture conditions in the course of the episode resulted in a new increase of discharge with its main peak exceeding 20 m³/s (I1 preliminary threshold), occurring on 0520 UTC 11 December. Then, the streamflow decreased gradually and stabilized below 2 m³/s after 1620 UTC 11 December (Figure 8). The above hydrometeorological conditions led to localized flooding in the Rafina stream basin with individual properties affected (I1 impact intensity class; Table 3).

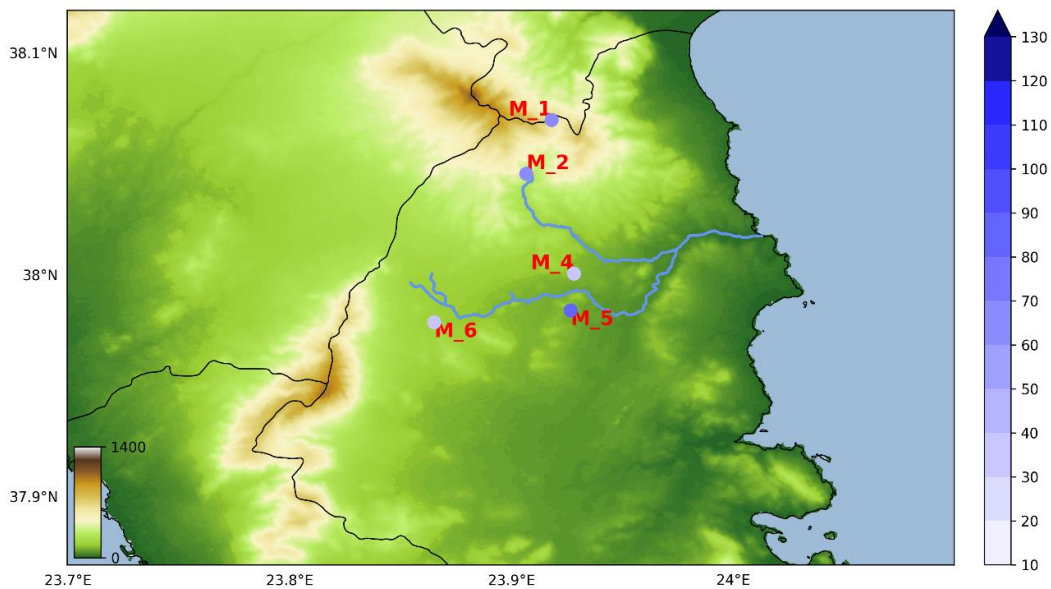


Figure 7. Topography of the study area and total accumulated rainfall observed in five meteorological stations during event #4 (10 December 2009, 2100 UTC to 11 December 2009, 0700 UTC).

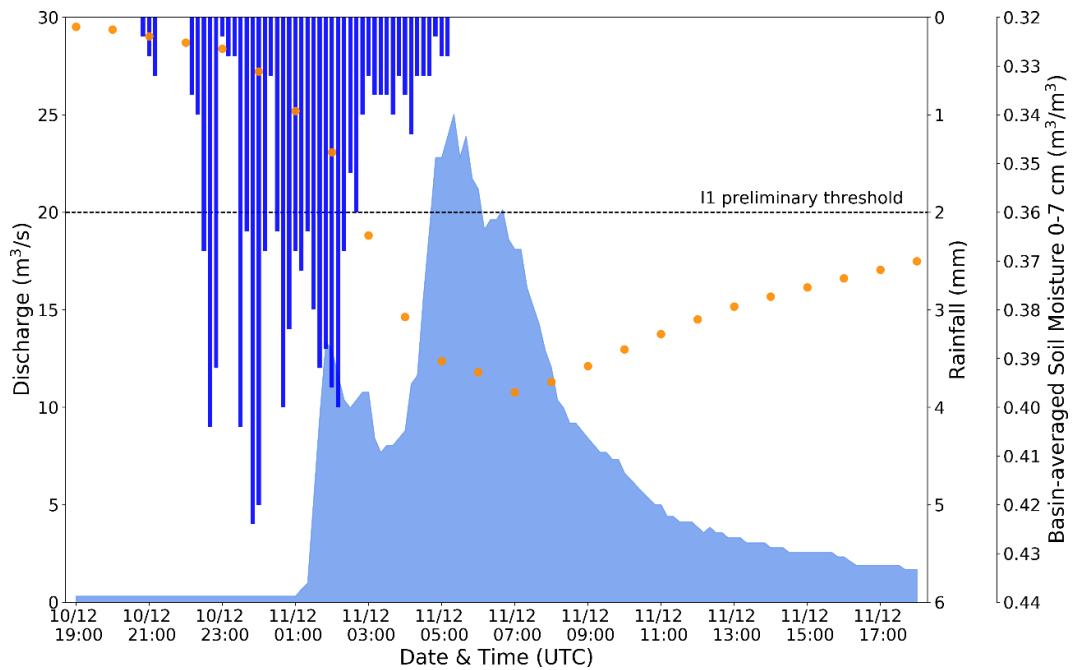


Figure 8. Timeseries of 10-min precipitation (blue bars; mm) and stream discharge (light blue filled areas; m³/s) over Spata meteorological station and Rafina hydrological station, respectively, and of 1-h basin-averaged volumetric (0–7 cm) soil water content (orange dots; m³/m³) from 10 December 2009, 1900 UTC, to 11 December 2009, 1800 UTC.

The precipitation in the study area during the examined episode was produced because of a surface low-pressure system, which developed in the Adriatic Sea (see location in Figure 1a) on 9 December and moved eastward across Greece during the next day (not shown). On 2200 UTC 10 December, the surface cyclone was located over the sea in southern Greece, close to the Crete island (see location in Figure 1a), along with a cut-off low at 500 hPa (Figure 9a,b). The very low air temperatures (less than $-26\text{ }^{\circ}\text{C}$; Figures 3b and 9d,f) and the high positive vorticity (more than $30 \times 10^{-5}\text{ s}^{-1}$; Figure A2a,b) that characterized the upper-level low, assisted the surface system to deepen and remain over the south maritime Greece during the next hours (Figures 3a and 9c,e). Thus, the intensification of the low-level convergence generated updrafts that led to the condensation of water vapour in the lower tropospheric layers (Figure A2c,d). As a result, strong near-surface northwest winds were induced over Attica, advecting warm and moist air to the plain area of the Rafina catchment, enhancing the atmospheric instability in the area, which caused the intense rainfall (Figure 8).

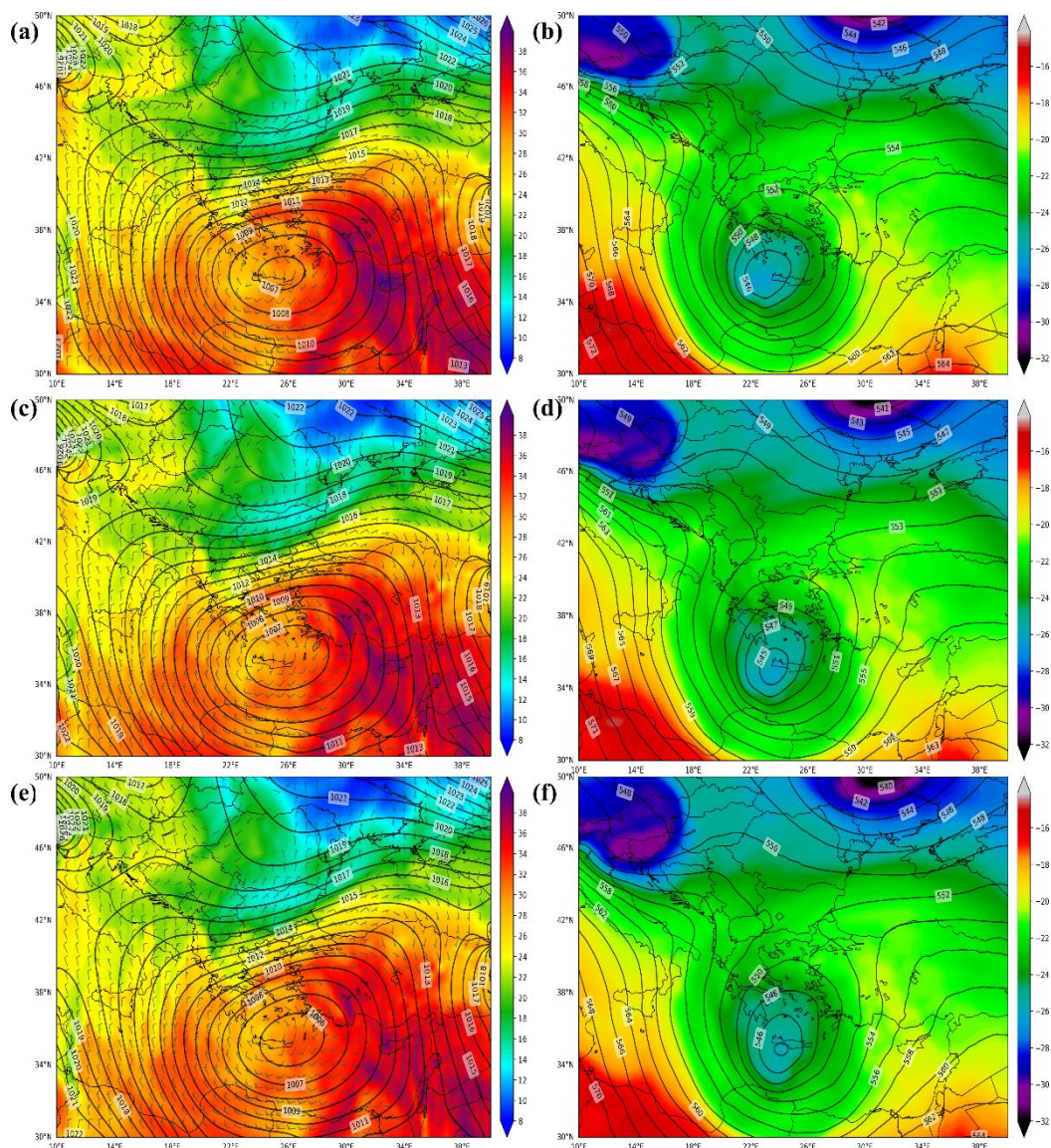


Figure 9. As in Figure 2 but for 10 December 2009, 2200 UTC (a,b), 11 December 2009, 0000 UTC (c,d), and 11 December 2009, 0200 UTC (e,f).

3.2.2. 22 February 2013

For episode #12, the highest values of total and 1-h rainfall were found at the Ayios Nikolaos (M_2) weather station, while the maximum stream discharge was observed at the Rafina hydrological monitoring site (see location in Figure 1b). More specifically, 138.8 mm of precipitation was recorded over Ayios Nikolaos from 0200 UTC to ~1100 UTC of 22 February, as illustrated in Figure 10. In the same short time period, the huge amounts of rainfall that fell in the Penteli Mountain region were also evident over the M_1 site (over 130 mm), whereas less than 30 mm of precipitation occurred in the monitoring stations located in the Spata plain (M_4, M_5 and M_6 sites).

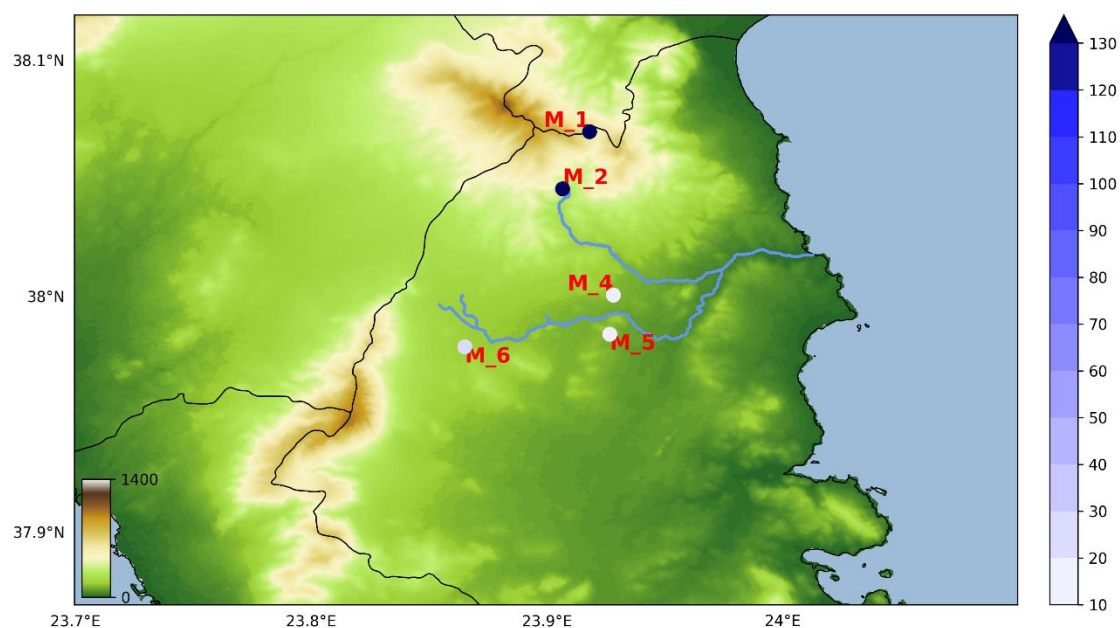


Figure 10. Topography of the study area and total accumulated rainfall observed in five meteorological stations during the event #12 (22 February 2013, 0200 UTC to 1100 UTC).

During the first three hours of rainfall over Ayios Nikolaos, a primary rainfall peak (7 mm at 0400 UTC) was observed, while high rainfall rates exceeding 10 mm were reported from 0500 UTC to 0630 UTC and from 0710 UTC to 0820 UTC, with the maximum 10-min record reaching up to 11.4 mm at 0740 UTC (Figure 11). The basin-averaged soil water content was higher than $0.38 \text{ m}^3/\text{m}^3$ before the storm's beginning, indicating a highly moist surface preconditioning, while the substantial 10-min rainfall amounts during the event led to peaks of soil moisture close to saturation (greater than $0.42 \text{ m}^3/\text{m}^3$) between 0600 UTC and 1100 UTC of 22 February. These conditions affected significantly the hydrologic response of the watershed, with the temporal profile of the streamflow at the Rafina station following the precipitation's temporal variations. In particular, the discharge began to increase at 0700 UTC, 5 h after the start of rain, with three peaks, which suppressed $20 \text{ m}^3/\text{s}$ (I1 preliminary threshold), occurring during three different periods. The maximum streamflow ($152.8 \text{ m}^3/\text{s}$) occurred at 1020 UTC, while its value fell below 60 and $40 \text{ m}^3/\text{s}$ (I2 preliminary threshold) after 1200 UTC and 1250 UTC, respectively (Figure 11). Significant impact (I2 impact intensity class; Table 3) was induced by the aforementioned hydrometeorological conditions, as, according to the Greek Fire Department (GFD) records, more than 10 operations related to flooded properties and public structures took place in Rafina-Pikermi municipality on 22 February 2013, while the GFD also operated for flood water pumping in the Pallini, Peania, Spata and Penteli regions.

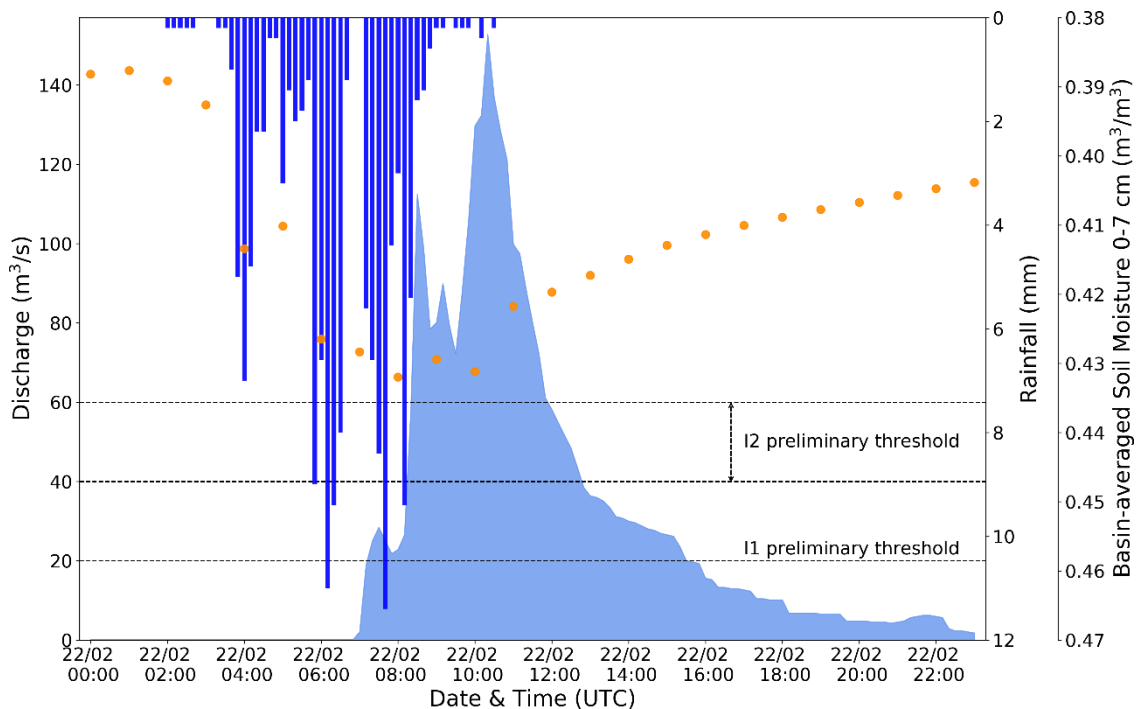


Figure 11. Time series of 10-min precipitation (blue bars; mm) and stream discharge (light blue filled areas; m^3/s) over Ayios Nikolaos meteorological station and Rafina hydrological station, respectively, and of 1-h basin-averaged volumetric (0–7 cm) soil water content (orange dots; m^3/m^3) from 10 December 2009, 1900 UTC, to 11 December 2009, 1800 UTC.

As already mentioned in Section 3.1, the key synoptic feature that led to the severe rainfall during event #12 was the evolution of the tilt of a middle-troposphere trough, which was related to a deep low-pressure system (mean sea-level pressure lower than 1003 hPa), a tilt that turned from positive to negative. This process occurred during the late-night hours of 21 February (not shown). On 0200 UTC 22 February, the negatively tilted 500-hPa through axis extended over the Ionian Sea with the surface low located west of the Crete island (see location in Figure 1a), while the system moved eastward during the next hours (Figure 12). These atmospheric conditions are associated with strong local instability, which in turn leads to intense convective activity that produces heavy storms [56]. This is evident during the examined episode, especially when the highest rainfall values were recorded over the area of interest around 0600 UTC and 0800 UTC of 22 February (Figure 11). At these times, the negatively tilted axis of the upper-level trough was positioned across the Rafina watershed (Figures 5f and 12f). As a result, highly unstable air masses with greater than 37°C (310 K) 850 hPa equivalent potential temperature (Figures 5e and 12e), 500–1000 J/kg convective available potential energy (CAPE) and lower than 100 J/kg convective inhibition (CIN; Figure A3a,b) were found over the study area. Consequently, deep and moist convection was developed, as shown by the high negative values of the vertically integrated moisture divergence (VIMD; Figure A3c,d) that indicate large moisture convergence, resulting in rainfall intensification. The development of strong convection, and the subsequent increase in precipitation, are also highlighted by the high positive vorticity band developed across the negatively tilted upper-level trough axis accompanied by a cloud-free zone across approximately the same area, indicating a dry intrusion in the middle troposphere (Figure A4). As noted by previous studies [56,57], these dry and high positive vorticity air masses penetrate into the warm and moist region ahead of the surface low, contributing to the enhancement of instability and convection. This feature is supported in the current study by the large number of lightning flashes detected by the NOAA ZEUS detection network between 0600 UTC and 0800 UTC of 22 February eastwards of the high positive vorticity band (Figure A5). Moreover, it is worth mentioning, that the highest total rainfall found over Ayios Nikolaos (M_2) and Diavasi Ballas

(M_1), indicates that convection may be enhanced by the topography and steep terrain slope in the north mountainous area (Mount Penteli) of the watershed (Figure 10), as also shown in previous studies (e.g., [54]).

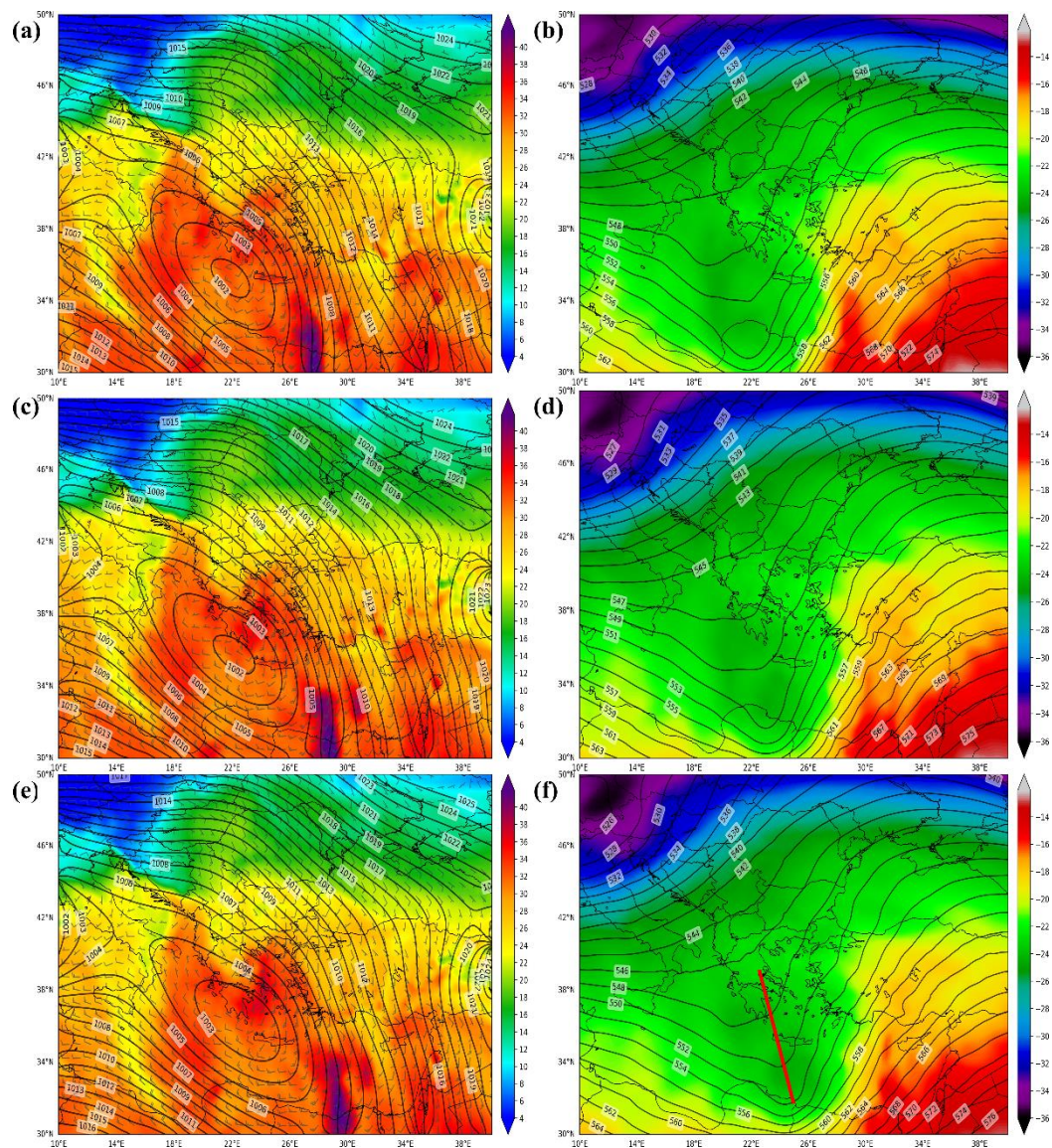


Figure 12. As in Figure 2 but for 22 February 2013, 0200 UTC (a,b), 0400 UTC (c,d) and 0600 UTC (e,f). The red line in map (f) indicates the negatively tilted trough axis.

4. Discussion—Concluding Remarks

The current work investigated, based on ground-based observations, ERA5 model reanalysis data and impact reports and records, the hydrometeorological characteristics and socio-economic impact of 12 stream flood events that occurred from 2008 to 2014 in the Rafina watershed in Attica, Greece, which is one of the three targeted catchments where a pilot flood forecasting system will be developed and validated in the framework of the CyFFORS project. The analysis revealed that most episodes were related to a typical, for the examined area, wet-season cyclonic atmospheric activity leading mainly to minor impact. The flood-related impact was significant for two events, namely #6 and #12, which occurred on February 2011 and 2013, respectively, and were associated with exceptional synoptic-scale weather conditions. Low rainfall amounts were recorded for several hours during the first episode resulting in a great total accumulation of precipitation, while high-intensity rainfall in

a short period characterized the second flood. Overall, positive relationships characterized by high correlations were found between the observed peak discharge and the duration and maximum total accumulation of rainfall. Moreover, a strong positive correlation between the peak stream discharge and flooding impact was evident, while the same outcome applied also for the maximum stream discharge and 1-h precipitation, when the events #6 and #9 were excluded from the analysis.

The above findings show that precipitation monitoring in the Rafina catchment, which is characterized as adequate in terms of spatial distribution of rain gauges, can assist in the characterization of a storm's potential to contribute to flood generation and, thus, provide generalized warnings. Location-specific flood alerts can be issued according to socio-economic impact-based streamflow thresholds. The present analysis provided some preliminary results in this direction. In particular, minimal impact was reported when the peak discharge was lower than 20 m³/s (I1 preliminary threshold). Maximum stream discharges that ranged from 20 m³/s to 40 m³/s were associated with minor impact, while significant impact was induced by events that were characterized by peak stream flows higher than 40–60 m³/s (I2 preliminary threshold). It should be noted that the reliability of the derived thresholds is moderated by the analysis limitations related to the lack of discharge data at all the locations at risk along the Rafina stream. However, they can be used primarily during the pilot operational application of the river/stream flood forecasting system in the framework of the CyFFORS project. The preliminary discharge thresholds will be evaluated, and possibly revised, based on future modeling data and analysis.

The detailed investigation of two case studies that occurred on 11 December 2009 (event #4) and 22 February 2013 (event #12), unraveled spatial and temporal differences in the generation and development of the rainfall, as well as in soil water content conditions, and the accompanying flooding. In the course of event #4, which led to minor impact (I1 impact intensity class; Table 3), the weather forcing resulted in the recording of maximum precipitation over Spata_M. Consequently, the small low-slope streams of Spata plain (see location in Figure 1b) contributed mainly to the hydrological response of the main Rafina stream, which was also determined by the considerable basin-averaged soil moisture values that varied from ~0.32 m³/m³ to ~0.39 m³/m³ prior to, and during, the episode. In contrast, the atmospheric conditions, which interacted with the topography, during event #12 that resulted in significant impact (I2 impact intensity class; Table 3), led to enhanced convection and to the occurrence of the highest rainfall values over Ayios Nikolaos, affecting an already highly moist surface (soil moisture range prior to and during the episode: 0.38–0.43 m³/m³) in the basin. As a result, the hydrological response of the main Rafina stream originated from the small steep-terrain streams of Mount Penteli (see location in Figure 1b) with both saturation and infiltration excess contributing to flooding. The aforementioned outcomes highlight the importance of the spatiotemporal variability of the flood-related storms' forcing mechanisms and the need for operationally monitoring and forecasting these mechanisms. They also demonstrate the significant role of soil moisture preconditioning in the magnitude of flooding and in the intensity of the resulting socio-economic impacts. For this, the simulation of soil water content and associated indices (e.g., soil moisture deficit) will be considered during the pilot operational application of the CyFFORS flood forecasting system.

Author Contributions: Conceptualization, C.G., V.K., K.L., C.O., H.H. and K.P.; methodology, C.G., V.K., K.L., C.O.; software, C.G.; validation, C.G., V.K., K.L., C.O.; formal analysis, C.G.; investigation, C.G.; resources, V.K., K.L.; data curation, C.G. and K.P.; writing—original draft preparation, C.G.; writing—review and editing, C.G., V.K., K.L., C.O., H.H. and K.P.; visualization, C.G.; supervision, V.K., K.L., C.O.; project administration, C.O.; funding acquisition, C.G., V.K., K.L., C.O., H.H. All authors have read and agreed to the published version of the manuscript.

Funding: This study was funded by the project Cyprus Flood Forecasting System—POST-DOC/0718/0040 which is co-funded by the Republic of Cyprus and the European Regional Development Fund (through the 'DIDAKTOR' RESTART 2016–2020 Programme for Research, Technological Development and Innovation).

Acknowledgments: The hydrometeorological data in nine stations in the Rafina stream basin were derived from the Hydrological Observatory of Athens (HOA) operated by the National Technical University of Athens (NTUA; <http://hoa.ntua.gr/>). Additional hydrological data in one of these stations (Lykorema) were kindly provided by E. Baltas (NTUA).

Conflicts of Interest: The authors declare no conflict of interest.

Appendix A

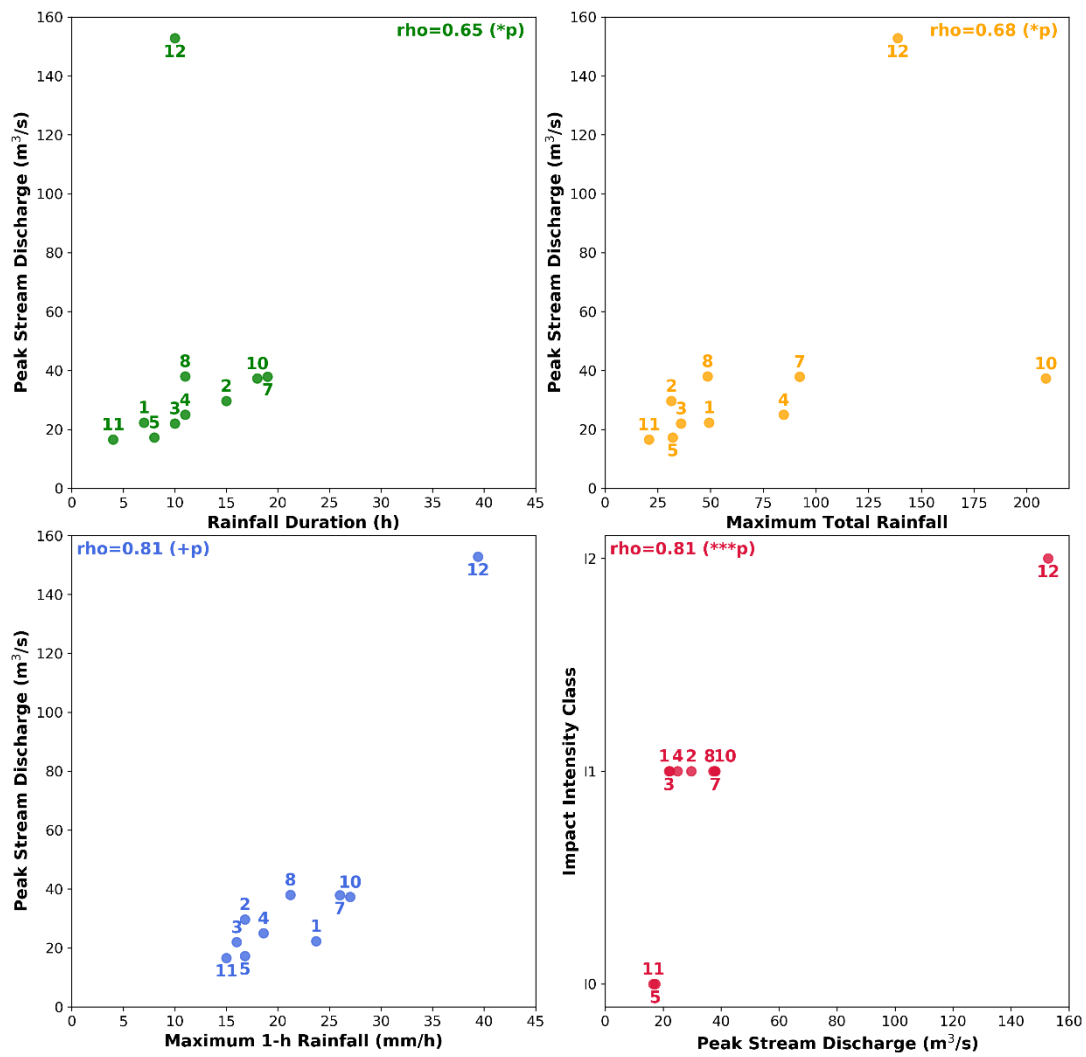


Figure A1. As in Figure 2 but without considering the events #6 and #9 in the analysis. The numbers indicate the events IDs (Table 3), while rho values indicate the Spearman correlation coefficient, with statistical significance, p value, being symbolized as: + p (>0.05 ; not significant), * p (≤ 0.05 ; 95% confidence interval) and *** p (<0.001 ; 99.9% confidence interval).

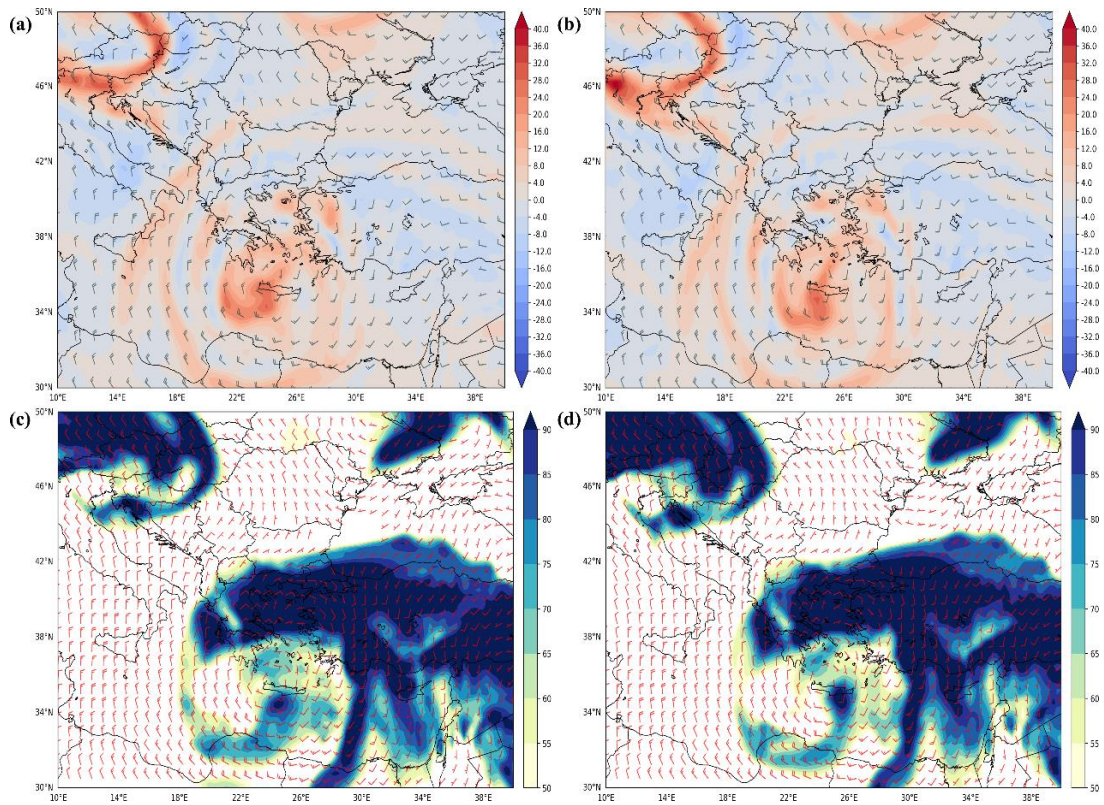


Figure A2. 500 hPa relative vorticity (shading; 10^{-5} s^{-1}) and wind bars (a,b), and 700 hPa relative humidity (shading; %) and wind bars (c,d) from the $0.25^\circ \times 0.25^\circ$ ERA5 reanalysis data on 11 December 2009, 0000 UTC (a,c) and 0200 UTC (b,d).

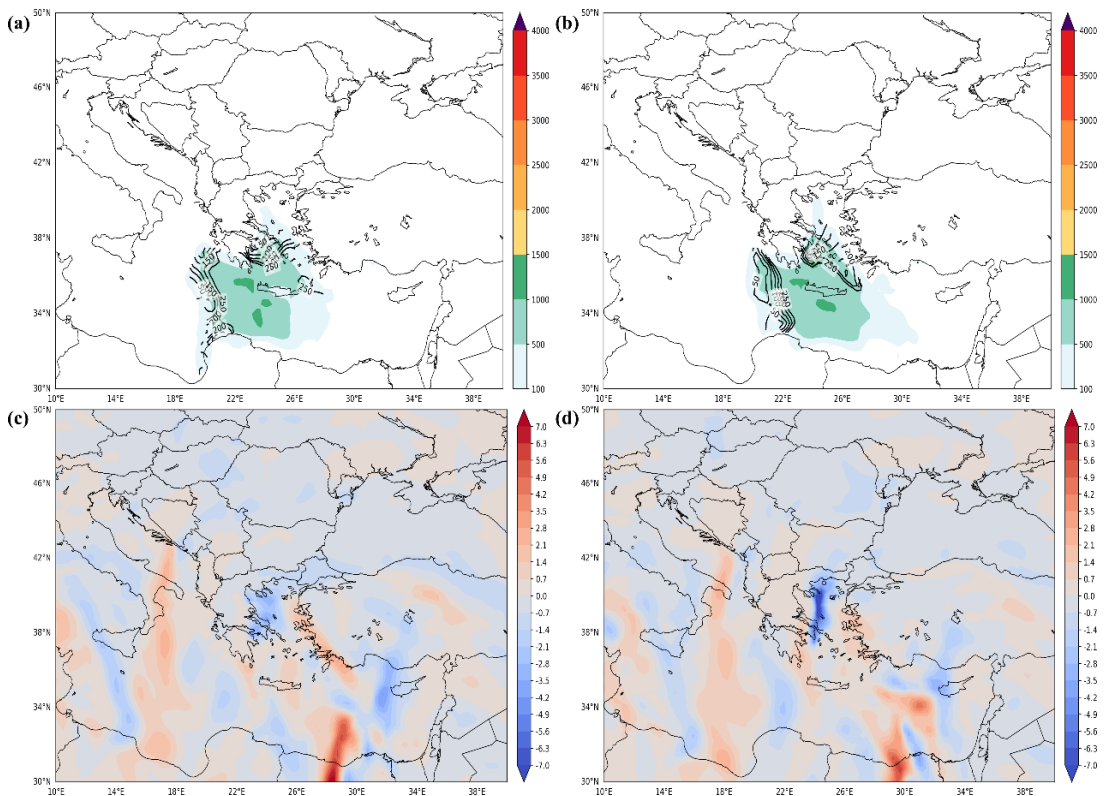


Figure A3. CAPE (shading; J kg^{-1}) and CIN (contours; J kg^{-1} ; a,b), and VIMD (kg m^{-2} ; c,d) from the $0.25^\circ \times 0.25^\circ$ ERA5 reanalysis data on 22 February 2013, 0600 UTC (a,c) and 0800 UTC (b,d).

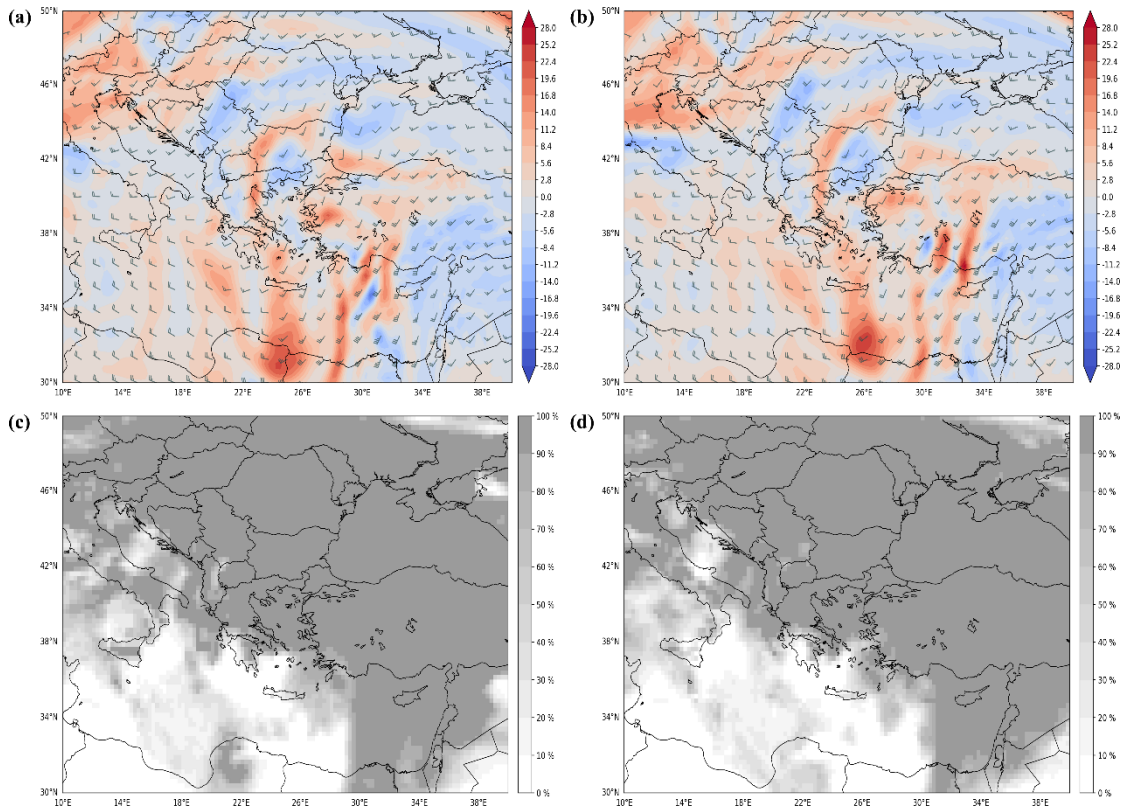


Figure A4. 500 hPa relative vorticity (shading; 10^{-5} s^{-1}) and wind barbs (a,b), and total cloud cover (c,d) from the $0.25^\circ \times 0.25^\circ$ ERA5 reanalysis data on 22 February 2013, 0600 UTC (a,c) and 0800 UTC (b,d).

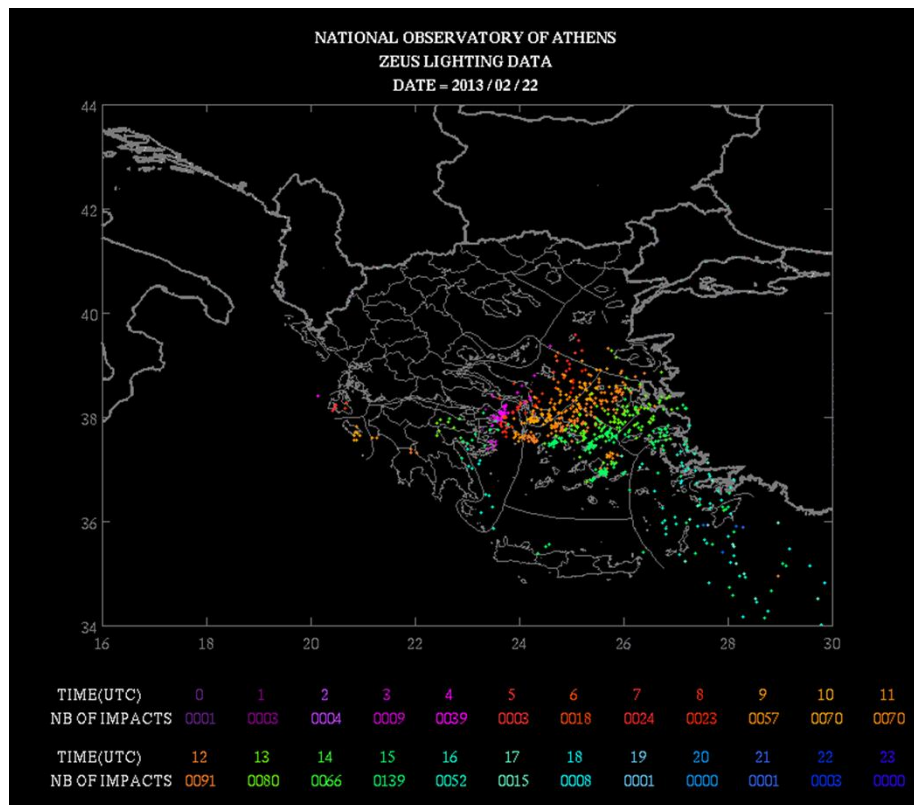


Figure A5. NOA ZEUS lightning data over Greece on 22 February 2013.

References

1. Hoeppe, P. Trends in weather related disasters—Consequences for insurers and society. *Weather Clim. Extrem.* **2016**, *11*, 70–79. [[CrossRef](#)]
2. Diakakis, M.; Boufidis, N.; Salanova Grau, J.M.; Andreadakis, E.; Stamos, I. A systematic assessment of the effects of extreme flash floods on transportation infrastructure and circulation: The example of the 2017 Mandra flood. *Int. J. Disaster Risk Reduct.* **2020**, *47*, 101542. [[CrossRef](#)]
3. Diakakis, M.; Andreadakis, E.; Nikolopoulos, E.I.; Spyrou, N.I.; Gogou, M.E.; Deligiannakis, G.; Katsetsiadou, N.K.; Antoniadis, Z.; Melaki, M.; Georgakopoulos, A.; et al. An integrated approach of ground and aerial observations in flash flood disaster investigations. The case of the 2017 Mandra flash flood in Greece. *Int. J. Disaster Risk Reduct.* **2019**, *33*, 290–309. [[CrossRef](#)]
4. Varlas, G.; Anagnostou, M.N.; Spyrou, C.; Papadopoulos, A.; Kalogiros, J.; Mentzafou, A.; Michaelides, S.; Baltas, E.; Karymbalis, E.; Katsafados, P. A multi-platform hydrometeorological analysis of the flash flood event of 15 November 2017 in Attica, Greece. *Remote Sens.* **2019**, *11*, 45. [[CrossRef](#)]
5. Bissolli, P.; Friedrich, K.; Rapp, J.; Ziese, M. Flooding in eastern central Europe in May 2010 - Reasons, evolution and climatological assessment. *Weather* **2011**, *66*, 147–153. [[CrossRef](#)]
6. Cojoc, G.M.; Romanescu, G.; Tirnovan, A. Exceptional floods on a developed river: Case study for the Bistrita River from the Eastern Carpathians (Romania). *Nat. Hazards* **2015**, *77*, 1421–1451. [[CrossRef](#)]
7. Kundzewicz, Z.W.; Ulbrich, U.; Brücher, T.; Graczyk, D.; Krüger, A.; Leckebusch, G.C.; Menzel, L.; Pińskwar, I.; Radziejewski, M.; Szwed, M. Summer Floods in Central Europe—Climate Change Track? *Nat. Hazards* **2005**, *36*, 165–189. [[CrossRef](#)]
8. Lorenzo-Lacruz, J.; Amengual, A.; Garcia, C.; Morán-Tejeda, E.; Homar, V.; Maimó-Far, A.; Hermoso, A.; Ramis, C.; Romero, R. Hydro-meteorological reconstruction and geomorphological impact assessment of the October 2018 catastrophic flash flood at Sant Llorenç, Mallorca (Spain). *Nat. Hazards Earth Syst. Sci.* **2019**, *19*, 2597–2617. [[CrossRef](#)]
9. Papagiannaki, K.; Lagouvardos, K.; Kotroni, V. A database of high-impact weather events in Greece: A descriptive impact analysis for the period 2001–2011. *Nat. Hazards Earth Syst. Sci.* **2013**, *13*, 727–736. [[CrossRef](#)]
10. Papaioannou, G.; Varlas, G.; Terti, G.; Papadopoulos, A.; Loukas, A.; Panagopoulos, Y.; Dimitriou, E. Flood inundation mapping at ungauged basins using coupled hydrometeorological-hydraulic modelling: The catastrophic case of the 2006 Flash Flood in Volos City, Greece. *Water* **2019**, *11*, 2328. [[CrossRef](#)]
11. Vinet, F.; Bigot, V.; Petrucci, O.; Papagiannaki, K.; Llasat, M.C.; Kotroni, V.; Boissier, L.; Aceto, L.; Grimalt, M.; Llasat-Botija, M.; et al. Mapping flood-related mortality in the mediterranean basin. Results from the MEFF v2.0 DB. *Water* **2019**, *11*, 2196. [[CrossRef](#)]
12. Gaume, E.; Borga, M.; Llassat, M.C.; Maouche, S.; Gaume, E.; Borga, M.; Llassat, M.C.; Maouche, S.; Lang, M. Mediterranean extreme floods and flash floods. In *The Mediterranean Region under Climate Change. A Scientific Update*; IRD Editions: Marseille, France, 2017; pp. 133–144.
13. Kotroni, V.; Lagouvardos, K. Lightning in the Mediterranean and its relation with sea-surface temperature. *Environ. Res. Lett.* **2016**, *11*, 34006. [[CrossRef](#)]
14. Michaelides, S.; Karacostas, T.; Sánchez, J.L.; Retalis, A.; Pytharoulis, I.; Homar, V.; Romero, R.; Zanis, P.; Giannakopoulos, C.; Bühl, J.; et al. Reviews and perspectives of high impact atmospheric processes in the Mediterranean. *Atmos. Res.* **2018**, *208*, 4–44. [[CrossRef](#)]
15. Seneviratne, S.I.; Nicholls, N.; Easterling, D.; Goodess, C.M.; Kanae, S.; Kossin, J.; Luo, Y.; Marengo, J.; McInnes, K.; Rahimi, M.; et al. Changes in climate extremes and their impacts on the natural physical environments. In *Managing the Risks of Extreme Events and Disasters to Advance Climate Change Adaptation. A Special Report of Working Groups I and II of the Intergovernmental Panel on Climate Change*; Cambridge University Press: Cambridge, NY, USA, 2012; pp. 109–230.
16. Alfieri, L.; Burek, P.; Feyen, L.; Forzieri, G. Global warming increases the frequency of river floods in Europe. *Hydrol. Earth Syst. Sci.* **2015**, *19*, 2247–2260. [[CrossRef](#)]
17. Dottori, F.; Szewczyk, W.; Ciscar, J.-C.; Zhao, F.; Alfieri, L.; Hirabayashi, Y.; Bianchi, A.; Mongelli, I.; Frieler, K.; Betts, R.A.; et al. Increased human and economic losses from river flooding with anthropogenic warming. *Nat. Clim. Chang.* **2018**, *8*, 781–786. [[CrossRef](#)]

18. Koks, E.E.; Thissen, M.; Alfieri, L.; De Moel, H.; Feyen, L.; Jongman, B.; Aerts, J.C.J.H. The macroeconomic impacts of future river flooding in Europe. *Environ. Res. Lett.* **2019**, *14*, 084042. [[CrossRef](#)]
19. Winsemius, H.C.; Aerts, J.C.J.H.; van Beek, L.P.H.; Bierkens, M.F.P.; Bouwman, A.; Jongman, B.; Kwadijk, J.C.J.; Ligtoet, W.; Lucas, P.L.; van Vuuren, D.P.; et al. Global drivers of future river flood risk. *Nat. Clim. Chang.* **2016**, *6*, 381–385. [[CrossRef](#)]
20. Gochis, D.J.; Barlage, M.; Dugger, A.; FitzGerald, K.; Karsten, L.; McAllister, M.; McCreight, J.; Mills, J.; RafieeiNasab, A.; Read, L.; et al. *The WRF-Hydro Modeling System Technical Description, (Version 5.0)*; NCAR Technical Note: Boulder, CO, USA, 2018.
21. Skamarock, W.C.; Klemp, J.B.; Dudhia, J.; Gill, D.O.; Liu, Z.; Berner, J.; Wang, W.; Powers, J.G.; Duda, M.G.; Barker, D.M.; et al. *A Description of the Advanced Research WRF Model Version 4*; NCAR Technical Note: Boulder, CO, USA, 2019.
22. Avolio, E.; Federico, S.; Miglietta, M.M.; Lo Feudo, T.; Calidonna, C.R.; Sempreviva, A.M. Sensitivity analysis of WRF model PBL schemes in simulating boundary-layer variables in southern Italy: An experimental campaign. *Atmos. Res.* **2017**, *192*, 58–71. [[CrossRef](#)]
23. Galanaki, E.; Lagouvardos, K.; Kotroni, V.; Giannaros, T.; Giannaros, C. Implementation of WRF-Hydro at two drainage basins in the region of Attica, Greece. *Nat. Hazards Earth Syst. Sci. Discuss.* **2020**, *2020*, 1–28.
24. Givati, A.; Gochis, D.; Rummeler, T.; Kunstmann, H. Comparing One-Way and Two-Way Coupled Hydrometeorological Forecasting Systems for Flood Forecasting in the Mediterranean Region. *Hydrology* **2016**, *3*, 19. [[CrossRef](#)]
25. Gochis, D.J.; Dugger, A.; McCreight, J.; Karsten, L.R.; Logan, Y.W.; Pan, L.; Yates, D.; Zhang, Y.; Sampson, K.; Cosgrove, B.; et al. *Technical Description of the National Water Model Implementation of WRF-Hydro*; Technical Report; Consortium of Universities for the Advancement of Hydrologic Science (CUAHSI): Cambridge, MA, USA, 2016.
26. Ryu, Y.; Lim, Y.-J.; Ji, H.-S.; Park, H.-H.; Chang, E.-C.; Kim, B.-J. Applying a coupled hydrometeorological simulation system to flash flood forecasting over the Korean Peninsula. *Asia Pac. J. Atmos. Sci.* **2017**, *53*, 421–430. [[CrossRef](#)]
27. Hunt, K.M.R.; Menon, A. The 2018 Kerala floods: A climate change perspective. *Clim. Dyn.* **2020**, *54*, 2433–2446. [[CrossRef](#)]
28. Xue, Z.G.; Gochis, D.J.; Yu, W.; Keim, B.D.; Rohli, R.V.; Zang, Z.; Sampson, K.; Dugger, A.; Sathiaraj, D.; Ge, Q. Modeling Hydroclimatic Change in Southwest Louisiana Rivers. *Water* **2018**, *10*, 596. [[CrossRef](#)]
29. Borga, M.; Boscolo, P.; Zanon, F.; Sangati, M. Hydrometeorological Analysis of the 29 August 2003 Flash Flood in the Eastern Italian Alps. *J. Hydrometeorol.* **2007**, *8*, 1049–1067. [[CrossRef](#)]
30. Delrieu, G.; Nicol, J.; Yates, E.; Kirstetter, P.-E.; Creutin, J.-D.; Anquetin, S.; Obled, C.; Saulnier, G.-M.; Ducrocq, V.; Gaume, E.; et al. The Catastrophic Flash-Flood Event of 8–9 September 2002 in the Gard Region, France: A First Case Study for the Cévennes–Vivarais Mediterranean Hydrometeorological Observatory. *J. Hydrometeorol.* **2005**, *6*, 34–52. [[CrossRef](#)]
31. Ruin, I.; Creutin, J.-D.; Anquetin, S.; Lutoff, C. Human exposure to flash floods – Relation between flood parameters and human vulnerability during a storm of September 2002 in Southern France. *J. Hydrol.* **2008**, *361*, 199–213. [[CrossRef](#)]
32. Pino, D.; Ruiz-Bellet, J.L.; Balasch, J.C.; Romero-León, L.; Tuset, J.; Barriendos, M.; Mazon, J.; Castellort, X. Meteorological and hydrological analysis of major floods in NE Iberian Peninsula. *J. Hydrol.* **2016**, *541*, 63–89. [[CrossRef](#)]
33. Greco, A.; De Luca, D.L.; Avolio, E. Heavy Precipitation Systems in Calabria Region (Southern Italy): High-Resolution Observed Rainfall and Large-Scale Atmospheric Pattern Analysis. *Water* **2020**, *12*, 1468. [[CrossRef](#)]
34. Pelosi, A.; Furcolo, P.; Rossi, F.; Villani, P. The characterization of extraordinary extreme events (EEEs) for the assessment of design rainfall depths with high return periods. *Hydrol. Process.* **2020**, *34*, 2543–2559. [[CrossRef](#)]
35. Romang, H.; Zappa, M.; Hilker, N.; Gerber, M.; Dufour, F.; Frede, V.; Béro, D.; Oplatka, M.; Hegg, C.; Rhyner, J. IFKIS-Hydro: An early warning and information system for floods and debris flows. *Nat. Hazards* **2011**, *56*, 509–527. [[CrossRef](#)]
36. Cole, S.J.; Moore, R.J.; Wells, S.C.; Mattingley, P.S. Real-time forecasts of flood hazard and impact: Some UK experiences. *E3S Web Conf.* **2016**, *7*, 18015. [[CrossRef](#)]

37. Silvestro, F.; Rossi, L.; Campo, L.; Parodi, A.; Fiori, E.; Rudari, R.; Ferraris, L. Impact-based flash-flood forecasting system: Sensitivity to high resolution numerical weather prediction systems and soil moisture. *J. Hydrol.* **2019**, *572*, 388–402. [CrossRef]
38. Hersbach, H.; Bell, B.; Berrisford, P.; Hirahara, S.; Horányi, A.; Muñoz-Sabater, J.; Nicolas, J.; Peubey, C.; Radu, R.; Schepers, D.; et al. The ERA5 global reanalysis. *Q. J. R. Meteorol. Soc.* **2020**, *146*, 1999–2049. [CrossRef]
39. Special Secretariat of Water, Ministry of Environment and Energy, Greece. *Flood risk management plan for the Attica Hydrological Region River Basins, Stage I, 1st Phase—Deliverable 1, Analysis of the Areas' Features and Flood Mechanisms*; The Hellenic Government: Athens, Greece, 2017.
40. The European Parliament and the Council of the European Union. Directive 2007/60/EC on the assessment and management of flood risks. *Off. J. Eur. Union* **2007**, *288*, 27–34.
41. Lagouvardos, K.; Kotroni, V.; Bezes, A.; Koletsis, I.; Kopania, T.; Lykoudis, S.; Mazarakis, N.; Papagiannaki, K.; Vougioukas, S. The automatic weather stations NOANN network of the National Observatory of Athens: Operation and database. *Geosci. Data J.* **2017**, *4*, 4–16. [CrossRef]
42. Papathanasiou, C.; Makropoulos, C.; Baltas, E.; Mimikou, M. The Hydrological observatory of Athens: A state-of-the-art network for the assessment of the hydrometeorological regime of Attica. In Proceedings of the 13th International Conference on Environmental Science and Technology, Athens, Greece, 5–7 September 2013.
43. Copernicus Climate Change Service (C3S) (2017): ERA5: Fifth Generation of ECMWF Atmospheric Reanalyses of the Global Climate. Copernicus Climate Change Data Store (CDS). ERA5 Hourly Data on Single Levels from 1979 to Present. Available online: <https://cds.climate.copernicus.eu/cdsapp#!/dataset/reanalysis-era5-single-levels?tab=overview> (accessed on 8 August 2020). [CrossRef]
44. Copernicus Climate Change Service (C3S) (2017): ERA5: Fifth Generation of ECMWF Atmospheric Reanalyses of the Global Climate. Copernicus Climate Change Data Store (CDS). ERA5 Hourly Data on Pressure Levels from 1979 to Present. Available online: <https://cds.climate.copernicus.eu/cdsapp#!/dataset/10.24381/cds.bd0915c6?tab=overview> (accessed on 8 August 2020). [CrossRef]
45. Kotroni, V.; Lagouvardos, K. Lightning occurrence in relation with elevation, terrain slope, and vegetation cover in the Mediterranean. *J. Geophys. Res. Atmos.* **2008**, *113*, D21. [CrossRef]
46. Lagouvardos, K.; Kotroni, V.; Betz, H.-D.; Schmidt, K. A comparison of lightning data provided by ZEUS and LINET networks over Western Europe. *Nat. Hazards Earth Syst. Sci.* **2009**, *9*, 1713–1717. [CrossRef]
47. Papagiannaki, K.; Lagouvardos, K.; Kotroni, V.; Bezes, A. Flash flood occurrence and relation to the rainfall hazard in a highly urbanized area. *Nat. Hazards Earth Syst. Sci.* **2015**, *15*, 1859–1871. [CrossRef]
48. Flood Forecasting Centre. *Flood Guidance Statement User Guide*; Flood Forecasting Centre: London, UK, 2020.
49. Speight, L.; Cole, S.J.; Moore, R.J.; Pierce, C.; Wright, B.; Golding, B.; Cranston, M.; Tavendale, A.; Dhondia, J.; Ghimire, S. Developing surface water flood forecasting capabilities in Scotland: An operational pilot for the 2014 Commonwealth Games in Glasgow. *J. Flood Risk Manag.* **2018**, *11*, S884–S901. [CrossRef]
50. Copernicus Climate Change Service (C3S) (2017): ERA5: Fifth Generation of ECMWF Atmospheric Reanalyses of the Global Climate. Copernicus Climate Change Data Store (CDS). ERA5-Land Hourly Data from 1981 to Present. Available online: <https://cds.climate.copernicus.eu/cdsapp#!/dataset/10.24381/cds.e2161bac?tab=overview> (accessed on 8 August 2020). [CrossRef]
51. Diakakis, M. Flood seasonality in Greece and its comparison to seasonal distribution of flooding in selected areas across southern Europe. *J. Flood Risk Manag.* **2017**, *10*, 30–41. [CrossRef]
52. Giannaros, C.; Kotroni, V.; Lagouvardos, K.; Giannaros, M.T.; Pikridas, C. Assessing the Impact of GNSS ZTD Data Assimilation into the WRF Modeling System during High-Impact Rainfall Events over Greece. *Remote Sens.* **2020**, *12*, 383. [CrossRef]
53. Kotroni, V.; Lagouvardos, K.; Defer, E.; Dietrich, S.; Porcù, F.; Medaglia, C.M.; Demirtas, M. The Antalya 5 December 2002 Storm: Observations and Model Analysis. *J. Appl. Meteorol. Climatol.* **2006**, *45*, 576–590. [CrossRef]
54. Galanaki, E.; Kotroni, V.; Lagouvardos, K.; Argiriou, A. A ten-year analysis of cloud-to-ground lightning activity over the Eastern Mediterranean region. *Atmos. Res.* **2015**, *166*, 213–222. [CrossRef]
55. Lagouvardos, K.; Kotroni, V.; Dobricic, S.; Nickovic, S.; Kallos, G. The storm of October 21–22, 1994, over Greece: Observations and model results. *J. Geophys. Res. Atmos.* **1996**, *101*, 26217–26226. [CrossRef]

56. Lagouvardos, K.; Kotroni, V.; Defer, E. The 21–22 January 2004 explosive cyclogenesis over the Aegean Sea: Observations and model analysis. *Q. J. R. Meteorol. Soc.* **2007**, *133*, 1519–1531. [[CrossRef](#)]
57. Dafis, S.; Lagouvardos, K.; Kotroni, V.; Giannaros, T.M.; Bartzokas, A. Observational and modeling study of a mesoscale convective system during the HyMeX—SOP1. *Atmos. Res.* **2017**, *187*, 1–15. [[CrossRef](#)]



© 2020 by the authors. Licensee MDPI, Basel, Switzerland. This article is an open access article distributed under the terms and conditions of the Creative Commons Attribution (CC BY) license (<http://creativecommons.org/licenses/by/4.0/>).